Accepted Manuscript

Morphology, internal structure and formation of ice ridges in the sea around Svalbard

Victoria Bonath, Chris Petrich, Bjørnar Sand, Lennart Fransson, Andrzej Cwirzen

PII: S0165-232X(17)30313-0
DOI: doi:10.1016/j.coldregions.2018.08.011
Reference: COLTEC 2640

To appear in: *Cold Regions Science and Technology*

Received date: 6 July 2017
Revised date: 29 June 2018
Accepted date: 10 August 2018

Please cite this article as: Victoria Bonath, Chris Petrich, Bjørnar Sand, Lennart Fransson, Andrzej Cwirzen , Morphology, internal structure and formation of ice ridges in the sea around Svalbard. Coltec (2018), doi:10.1016/j.coldregions.2018.08.011

Morphology, Internal Structure and Formation of Ice Ridges in the Sea around Svalbard

Victoria Bonath[a*], Chris Petrich[b], Bjørnar Sand[b], Lennart Fransson[a], Andrzej Cwirzen[a]

[a]*Luleå University of Technology, 971 87 Luleå, Sweden*
[b]*Northern Research Institute Narvik, 8504 Narvik, Norway*
[*]*Corresponding author: victoria.bonath@ltu.se*

Victoria Bonath (corresponding author), Luleå Univ. of Technology, 971 87 Luleå, Sweden. (victoria.bonath@ltu.se) Phone number: +46 920 492934
Chris Petrich, Northern Research Institute, P.O. Box 250, 8504 Narvik, Norway. (christian.petrich@norut.no)
Bjørnar Sand, Northern Research Institute, P.O. Box 250, 8504 Narvik. (bjoernar.sand@norut.no)
Lennart Fransson, Luleå Univ. of Technology, 971 87 Luleå, Sweden. (lennart.fransson@ltu.se)
Andrzej Cwirzen, Luleå Univ. of Technology, 971 87 Luleå, Sweden. (andrzej.cwirzen@ltu.se)

Abstract

The results from 3 years of comprehensive field investigations on first-year ice ridges in the Arctic are presented in this paper. The scopes of these investigations were to fill existing knowledge gaps on ice ridges, gain understanding on ridge characteristics and study internal properties of ice. The ability of developing reliable simulations and load predictions for ridge-structure interactions is the final principal purpose, but beyond the scope of this paper. The presented data comprise ridge geometry, ice block dimensions from ridge sails, ice structure in the ridge and values on the ridge porosity and the degree of consolidation. The total ridge thickness conformed to other ridges studied in the same regions. The consolidated layer thickness was on average 2-3 times the level ice thickness. Minimum 33% and in average 90% of the ridge keel area was consolidated. The distribution of ice block sizes and block shapes within a ridge appears to be predictable. A new approach for deriving a possible ridging scenario and ridge age is presented. Different steps of the ridge building process were identified, which are in good agreement with earlier simulated ridging events. After formation of very thin lead ice between two floes deformation occurs through rafting and ridging until closure of the lead. Subsequently the adjacent level ice floe fractures proceeding ridge formation until ridging forces exceed driving forces. A time span of 10 days could be assessed for a possible ridge formation date, estimating the ridge age of the studied ridge located east of Edgeøya at 78° N to be 7 to 8 weeks.

Key words: First-year ice ridge; Ice block size; Ridge formation; Ridge Porosity; Ice texture

1 Introduction

A high potential for oil and gas resources in the Barents Sea attracts attention for future exploration. Beside the increase in petroleum activities and increased traffic due to petroleum activities, the Northern Sea Routes tend to get increasingly interesting for cargo ships. A trend to shrinkage of the arctic ice cap due to climate change will offer new prospects for shipping in the Northern Sea Routes. Yet harsh climate conditions and heavy sea ice features, such as sea ice ridges will persist as one of the major challenges that have to be mastered when operating in the Arctic. Even the Fram Strait, which is an outlet for sea ice from the arctic at high drift speeds, has future potential for more shipping activities (Smith and Stephenson, 2013). Sea ice ridges are frequently occurring ice phenomena. They form when two ice floes collide or shear and can create enormous piles of broken ice pieces. Freeze bonds between the ice blocks and refreezing of the part under the water surface turn sea ice ridges to robust ice features. First-year ridges, i.e. which are not older than one winter season, appear not only in high arctic regions, but also in more moderate climate conditions where human activities are prevalent. Sea ice ridges may be the main load scenario for the design of offshore-structures and ice-going vessels. To be able to predict load scenarios from ridges, geometrical and physical parameters have to be known. Therefore researchers concerned with ice actions on offshore structures and ships have studied pressure ridges in different arctic regions. Different obstacles were met that create difficulties for ridge characterization. Ridges have high variations in properties and shapes (Timco and Burden, 1997) and change throughout the season (Leppäranta et al., 1995). The accessibility to ridges is usually restricted and rough field conditions make it difficult to perform detailed or long-term field studies.

One approach to determine the strength and dimensions of pressure ridges is to study mechanical processes and energy balance of the ridge formation process. Ridge formation processes are difficult to observe in nature but several attempts were made to measure ridge-building forces in the 1990s. Based on the assumption that pack ice stresses of drifting ice floes are representative for ridge building forces, direct stress measurements showed stress levels varying from 24 $kN \cdot m^{-1}$ up to 1720 $kN \cdot m^{-1}$ (e.g., Nikitin and Kolesov, (1993); Comfort et al., (1998); Richter-Menge and Elder, (1998)).

Analytical and numerical models have been used to study the ridge building process. Parmerter and Coon (1972) used a one-dimensional analytical model to simulate the ridge building of two ice sheets moving towards each other with a lead filled with rubble. The appearance of the resulting ridges is similar to actual measured ridge geometries. A discrete element model presented in Hopkins (1994, 1998) assumes that initially a thin first-year ice floe moves towards a thick ice floe which is separated by lead. In addition to estimation of the energy consumption during ridge building, four different stages of the ridge formation were described (Hopkins, 1998). At first vertical sail growth is followed by vertical keel growth until maximum ridge draft is reached. In a third stage the keel growth continues towards the lead and may create a rubble field whereas stage four represents further compression of the rubble field. Ridge building can stop at any of the stages. Very little information is published on how ridge formation mechanism proceeds in nature, but it could be useful for verification of models describing the ridge building process. Tuhkuri and Lensu (2002) suggest from a series of ice tank tests that ridging is initiated by finger-rafting and rafting forces increase linearly with displacement followed by increasing ridging forces until the maximum ridging force is reached at the point where ridge growth only continues laterally.

Strub-Klein and Sudom (2012) established a database on all until then available ridge geometrical data from field investigations undertaken by different researchers. Different measurement techniques were summarized and their assets and drawbacks were discussed. Significant lacks of data were related to e.g. ice block dimensions, keel width and keel area as well as data on internal structure, physical and mechanical properties.

The internal structure of ridges, e.g. degree of consolidation or macro porosity, is difficult to access, but important for the understanding of ice ridges. The consolidated layer of a ridge is of interest since it is one of the main load components during first-year ridge-structure interactions according to ISO 19906 (2010). Considerable variations have been found so far (e.g. Timco and Burden, 1997, Høyland, 2007, Strub-Klein and Sudom, 2012) due to natural irregularities, uncertainties from measurement techniques and the lack of definition of the upper and lower boundary of the consolidated part. Ridge porosity is another important parameter used to model thermal processes within ridges (e.g. Høyland,

2002) and also to describe properties of the ice rubble (e.g. Hopkins and Hibler, 1991). Amundrud et al. (2006) found that high keel porosity enhances deterioration of the ice ridge. The compactness of the ice rubble and thus the ridge macroporosity (Surkov, 2001) is highly influenced by ice block dimensions and shapes. Hopkins and Hibler (1991) and Tuhkuri and Polojärvi (2005) showed that ice block shapes further affect the mechanical behavior of ice rubble. Hopkins et al. (1991) presented the influence of block shape, size and angularity on the energy required for ridging.

This paper provides comprehensive information on first-year sea ice ridges obtained from 3 years of field studies in arctic regions close to Svalbard. Information of first-year ridges especially from the Fram Strait and north-west of Svalbard is so far poor. The paper is composed of two parts:

- For the first time ridge profiles from both along the ridge spine and perpendicular to the ridge spine are presented. Ridge data from field measurements covering knowledge gaps on e.g. ridge cross-sectional area, ridge consolidation and block dimensions are presented and evaluated with regard to the state of the art. (Sections 3, 5.1 to 5.3).
- A recent approach is introduced for deriving a possible ridge formation scenario from the collected data in combination with climatic reanalysis data and widely recognized semi-empirical models on ice growth and ice drift (Section 4, 5.4).

2 Methods

2.1 Field and laboratory tests

Suitable ice ridge areas around Svalbard were identified at the start of the expedition through satellite images and reconnaissance flights performed by the Norwegian Coast Guard. The apparently largest ridges where selected within the chosen areas. The Norwegian Coast Guard vessel KV Svalbard was used for transport to ridge areas and the coast guard crew provided support for safety and manpower. In total 6 ice ridges were studied from 2011 to 2013. Ridge locations and surveying dates are given in Fig. 1 and Table 1.

The procedure for ridge measurements was as follows:

- Transects were staked along and across the ridge with a 5 meter distance between measuring points along the spine and 2 meter distance across the ridge.
- The surface topography of the ice was measured with a leveling telescope. The snow thickness on top of the ridge was measured by a yard stick.
- The keel depth and keel structure were estimated by mechanical drilling with a 50 mm auger. From the drilling resistance it was distinguished between hard ice, soft ice, slush and sections with no resistance. The two former categories were defined as ice and the two latter as a void.
- The direction of ice block thickness was identified visually based on ice fabric and orientation of brine channels. Ice block sizes were determined with a measuring tape. Inclination angles of the block side with the largest area were roughly estimated with the means of an equal-sided right triangle for identifying 45°, implying measurement errors of +/- 10°C. A block lying horizontally on the ice was 0° inclination.
- A sail width was defined as the widths where ice blocks were lying on the ice cover. The keel width was defined by the region between two fully refrozen ice covers with constant thickness. The keel width of R2-2013 could not readily be determined, because the keel probably merged with a not fully refrozen rubble field and the drillings were stopped without reaching level ice.
- The sail angles for the ridges in 2013 were measured in field by holding a pole forward, exactly horizontal from the sail top. At the end of the rod was a line with a weight that met the ridge at its foot. The horizontal and vertical distances resulted in a sail inclination angle using trigonometric functions for right-angled triangles. The remaining sail angels and all keel angles where calculated in almost the same manner, but taking the sail height and sail width and the keel depth and keel widths respectively from the measured profiles.

One cross-section was measured for each ridge from 2011 while for the ridges from 2012 and 2013 both a profile along the spine and one or two cross-sections were measured. For the ice blocks from 2011 and R1-2013 only thickness was available, whereas orientation and three dimensions of the blocks from all other ridges from 2012 and 2013 were determined. All measured ice blocks were from the ridge sails. Temperature profiles from the ridges and level ice were measured occasionally on 70 mm-diameter ice cores. Further mechanical and physical properties and the microstructure of the

ridges determined from 200 mm-diameter cores along the cross-sections are reported in Bonath et al. (in review). A study of horizontal and vertical thin sections under cross-polarized light from each ice core enabled determination of the ice texture.

2.2 Ridge Parameters

The definition according to ISO 19906 (2010) for characteristic ridge dimensions is used and outlined in Fig. 2. For clarification, the snow and slush layer usually prevailing on top of ice ridges are not considered in the values given for sail height H_s and sail area A_s. The sail area extends vertically from the uppermost ice to the water level and the keel area extends from the water level down to the lowermost ice. The consolidated part is defined as the solid ice part within the ice ridge and extends from the ice surface or below the loose sail rubble down to the unconsolidated keel rubble within the maximum keel width W_K. The lower boundary is defined as the first void below water level containing non-rigid material such as slush or seawater. Ice blocks are defined by the ice block thickness h_{bl}, the smallest (d_1) and largest (d_2) dimensions from the surface area A_{bl} and the inclination α_{bl}.

The internal structure of the ice ridges can be characterized by the macro porosity and the ice texture. The ice texture is characterized by crystal type and alignment of ice crystals. In the present study, ice is classified as columnar ice, granular ice or mixed ice (Richter-Menge and Cox, 1985).

Macroporosity (described by e.g. Høyland, 2002) was determined for both sail area, keel rubble and keel area including the consolidated layer (CL), as defined in Fig. 2. The macroporosity can be defined as the ratio of volume of voids within a ridge to the total ridge volume, Eq.1, where V_I is the ice volume, V_V is the volume of the voids and V is the total volume. The volume of voids comprises non-sea ice such as pores filled with air, water, snow or slush. The snow/slush layers on top of ridge sails are not accounted for in void volume.

$$\eta_M = 1 - \frac{V_I}{V} = \frac{V_V}{V} \qquad (1)$$

For the vertical macroporosity distribution, the volume of voids to the total volume at each depth interval is considered for all the boreholes corresponding to the depth. When the chosen depth interval exceeds the keel depth for a borehole, this borehole is excluded from the calculations.

2.3 Ridge Age

The method to re-construct the history of an ice ridge was described in detail by Petrich and Bonath (2014) and has been applied to ridge R2-2012. In this paper the drift track, age and formation process of ridge R3-2013 was analyzed.

Ice drift was estimated by a rule-of-thumb saying that sea ice moves proportional with the surface winds by factor 0.02 and 45° to the right of the wind direction (Colony and Thorndike, 1980). Free-drift approximation is realistic for ice fields with ice concentration lower than 80% (Leppäranta, 2011). It has to be kept in mind that local ice concentration can change rapidly to higher ice compactness. Thus limitations with free-drift approximations are the neglect of internal stresses and time varying ocean currents. The drift trajectory was iterated by wind data extracted from two reanalysis products: the National Centers for Environmental Prediction Climate Forecast System Version 2 (NCEP CFSV2, Kalnay et al., 1996), and the European Centre for Medium-Range Weather Forecasts (ECMWF) ERA-Interim (Dee et al., 2011). Reanalyzes for both air temperature and surface winds were produced every 6 hours from a T62 grid (NCEP) and a 0.5° x 0.5° grid (ERA-Interim) respectively.

The difference of block thickness and level ice thickness determines the ice growth since ridge formation, assuming that the surrounding level ice has resulted from undisturbed growth of the original level ice. From that the ridge age was ‘back-calculated’ by means of empirical equations for ice growth of sea ice based on Freezing Degree Days (FDD). Freezing Degree Days are defined in Eq. 2.

$$FDD = -\int (T_a - T_w)dt \qquad (2)$$

Where T_a is air temperature and T_w is the freezing temperature of water, which was assumed to be -1.8 °C for saline water. FDD are expressed in °C·days. Four different empirical FDD models shown in Eq. 3 to Eq. 6 were used and compared in this paper for doing ice growth calculations, where H (cm) is the ice thickness.

$$H^2 + 50H = 8FDD \text{ (Zubov, 1945)} \qquad (3)$$

$H^2 + 5.1H = 6.7FDD$ (Anderson, 1961) (4)

$H = 2FDD^{0.505}$ (Kovacs, 1996) (5)

$H^2 + 22H = 6.3FDD$ (Petrich and Eicken, 2010) (6)

3 Results

3.1 Field Measurements

3.1.1 Field observations from 2011

Two pressure ridges were surveyed at different locations in 2011. Ridge R1-2011 was located north of Svalbard in the Woodfjorden, in landfast ice (Fig.1; Table 1). Wet snow and slush covered the ice. The average snow thickness was 0.39 m, whereof the highest snow accumulations could be found at the sides of the ridge sail. The ridge was surrounded by level ice and ridge length did not exceed 30 m, Fig. 3a. The ridge cross-section shown in Fig. 3b appeared almost symmetrical and both sail and keel were triangular. The level ice thickness was 0.37 m on both sides of the ridge, i.e. the ridge formed from ice floes of equal thickness. The mean block thickness was 0.26 m. The consolidated layer could not be determined by drilling as the ice was generally very soft. Furthermore, the slush layer present on top of the ridge made it difficult to estimate whether slush or soft ice came up from the drill hole.

Ridge R2-2011 was located between Spitsbergen and Hopen Island. Weather conditions were slightly colder than for R1-2011. As shown in Fig. 4 the ridge length was not well defined since the ridge was a part of a network of deformations. A branched network was characteristic for the ice in the area. The average thickness of the level ice was 0.8 m which equaled the average sail block thickness.

3.1.2 Field observations from 2012

Only one ridge could be measured completely during 2012 due to very rough weather conditions. The work on ridge R1-2012 had to be stopped after bad weather approached. Air temperatures during both the R1-2012 and R2-2012 campaigns where mainly -20° or colder, but became milder during the day of measuring, up to -10°C. Overall the ice was very cold and brittle. The ridge was located in Fram Strait on an ice floe with size 200 m by 200 m. Several ridges where on the same floe. The spine of the

measured ridge R2-2012 was almost straight with a length of 25 m. Fig. 5 shows that the two transects perpendicular to the spine agreed well in shape, but transect B had a lower sail (by 0.6 m) and a deeper keel (by 3.4 m). The sail consisted of several big ice blocks with an average ice thickness of 0.87 m.

3.1.3 Field observations from 2013

The ridges in 2013 were all investigated east of Edgeøya in the end of April. The weather was consistently mild during this time, with air temperatures -5°C. This allowed for detailed investigation of ridge parameters for each ridge. Ridge R1-2013 had an S-curved ridge sail with a length of 100 m (Fig. 6b). The width of the triangular ridge sail reached a maximum of 14 m, with slope angles of 22° above the horizontal. The ridge keel was asymmetric, wide (32 m), and not particularly deep (maximum 3.4 m) compared to the sail, giving an H_k to H_s ratio as low as 1.5. The same ratio was recurring for all sail tops along the spine in Fig. 7a, which indicates some regularity throughout the ridge. The ridge was covered by a 0.3 m thick layer of snow at time of surveying, where most snow was located between 22 m and 38 m width of transect B in Fig. 7b. The average ice block thickness was 0.48 m and the thickness of the surrounding level ice was 0.7 m.

The shape of ridge R2-2013 was asymmetric with the sail top and maximum keel depth offset 10 m. Two transects were surveyed across the 65 m long ridge. Both transect gave similar results for shape, dimensions and consolidation. The whole ridge is covered by a 0.3 m snow layer. Wet snow was found on sail positions wider than 18 m, Fig. 8b. Transect B contained a wet layer in ice at 1 m depth that was apparent in ice cores taken at position 22 m to 28 m but appeared to have been missed during profile measurements. The consolidated layer thickness from 20 m to 32 m width was most probably caused by the missed wet layer, Fig. 8b. The level ice thickness on one side of R2-2013 was 0.6 m whereas it merged with a rubble-field on the other side. The block thickness was on average 0.4 m.

The shape of R3-2013, shown in Fig. 9, was similar to those observed in the case of the ridge R2-2013, Fig. 8. However, the ratio between the keel width and the sail width was higher for the ridge R3-2013, which resulted from a steep and narrow sail compared to a wide ridge keel. The offset between sail and keel maxima was 16 m. The ridge length exceeded the surveyed 120 m as can be seen from the aerial photo, Fig. 6. The average snow thickness was 0.2 m. More ridges and rubble fields were on the same floe as R3-2013.

Ice temperature profiles (Fig.10) measured in 2013 show consistently lower temperatures within the ridges compared to the surrounding level ice. For R1-2013 the temperature profile is measured throughout the keel depth. The uppermost point of each profile represents the air temperature, which was in most cases higher than measured ice temperatures during daytime (at time of measurement), but lower during the previous nights.

3.2 Macroporosity and consolidation

The average macroporosity was 13 % for ridge sails and 23 % for ridge keel rubble. Differences between ridges were large, ranging from 0 to 30 % and less than 1 up to 51 % for sails and keels, respectively. The ridge sails with zero porosity concerning the ridges from 2011 and 2012 consisted of only few ice blocks that either lay almost horizontally one top of each other with very few gaps or only one layer of ice blocks made up the sail. The ridge keel from R1-2013 was very flat with only small gaps between blocks which resulted in less than 1% of macroporosity.

The average consolidated layer thickness presented in Table 4 exceeded 1 m for all ridges. The consolidated layer was in general thicker along the spine of the ridges than along the perpendicular transects. The standard deviations of all profiles were between 0.5 and 1 times the consolidated layer thickness, thus a high variability for consolidated layer thickness within a ridge can be expected. The range between the maximum and minimum values of the consolidated layer thickness exceeded several meters for each evaluated profile. The consolidated layer was between 1.1 and 3.0 times thicker than the surrounding level ice.

3.3 Ice block dimensions

The ice block dimensions of in total 142 blocks from the ridge sails measured in 2012 and 2013 are summarized in Table 5. The histograms in Fig. 11 show one predominant ice block thickness, i.e. the modal block thickness for each ridge, which was 0.85 m for R2-2012. The modal block thicknesses for the ridges measured in 2013 were 0.45 m, 0.40 m and 0.25 m for R1-2013 to R3-2013 respectively, which nearly coincide with the average block thicknesses given in Table 5. The average block surface areas had no specific coherence with ice block thickness. The average ratio of block lengths d_2 and d_1

was 1.5. Average block inclination was with 50° much higher for the thinner blocks in 2013 than for the thick ice blocks with an average angle of 14° from the ridge measured in 2012.

4 Ridge Formation

4.1 Ice structure and ridge formation process

Ice cores with 20 cm diameter were taken in regular intervals along the measured cross-section B of R3-2013. Thin sections from the cores were studied for visualizing the internal structure of the ridge on a wider scale and to enable reconstruction of ridge formation process. Thin sections provided data related to thickness of the level ice at time of ridge formation and at time of field measurements, as well as block thickness and ridge internal structure, see Fig. 12. The ridge R3-2013 in Fig. 9 consisted of an over 120m long, irregularly spine (Fig. 6d), which is typical for compression ridges, Tucker et al. (1984). The geometry of the ridge cross-section was asymmetrical with a large ice block accumulation at keel widths exceeding 22 m and an offset between sail and keel maxima of 16 m. At width 0 m, the level ice was found to be 0.67 m thick. A thin section composite from level ice is shown in Fig. 12c (i). The upper 0.26 m of the level ice core resembled the fabric of ice blocks from the ridge sail, which was on average 0.26 m. This upper layer was found in all ice samples taken between 0 m and 16 m along the transect B, which indicates that the blocks originated from that floe and that this ice layer had not changed since ridge formation. From 25 m to 55 m in transect B the upper 0.50 to 0.60 m consisted of multiple rafted ice with ice layers being from 0.02 to 0.06 m thick , Fig. 12c (v). This was presumable a consequence of rafting, where a lead covered with a very thin ice layer started to close due to two converging ice sheets. Solely crushed ice was found close to the ridge sail (between 8 m and 16m) below the upper 0.26 m of the ice, below the ridge sail (between 16 m and 24 m) and below the rafted ice layer (until 42 m), Fig. 12c (iii). Crushed ice designates a refrozen ice mass, containing small ice fragments of different sizes and shapes, similar to mixed Type IIIA ice described by Richter-Menge and Cox (1985). The proposed ridge formation process is sketched in Fig. 12a to Fig. 12c. Firstly a 0.02 to 0.06 m thin ice cover formed in an open lead, Fig. 12a. The lead ice started with multiple rafting which was likely followed by ridging after being pushed by the ice floes. After the

lead ice is depleted, the ridge driving forces are strong enough that deformation continues with the adjacent 0.26 m thick ice floe, Fig. 12b. Fragments of thin ice in the keel indicate that crushed mixed ice within the keel could have been the lead ice. Else penetration of the level ice into the probably weaker pile of lead ice initiated the crushing of the ice in the keel. Intact ice blocks according to the thickness of the level ice sheet were found in both the ridge sail and the ridge keel.

4.2 Ice drift

Free drift theory was applied in order to assess how much the investigated ice may have moved during the ice growth period (Section 2.3). The drift paths generated from the NCEP and ERA-Interim wind data (Fig. 15) are almost congruent except for a time period in the beginning of February, where the NCEP drift track proceeds further north, close to Franz Josef Land, Fig. 13a and Fig. 13b.

Since free drift approximation is best applicable for single pieces of ice rather than for areas with packed ice, the plausibility of the drift path was verified with help of both ice charts from the Norwegian Meteorological Institute and daily quiver plots for ice drift, provided by the French Research Institute for Exploration of the Sea (CERSAT/IFREMER). Ice conditions along the drift path developed from open drift ice (40% to 90% ice concentration) in January, to close drift ice in February and March (70% to 90% ice concentration) and finally to close drift ice and very close drift ice (70% to 100% ice concentration) until end of April. From the examples shown in Fig. 13c, the calculated drift path follows the ice drift trajectoris produced by IFREMER. Hence, under free-drift assumptions, the ridges formed most probably within 10° to 15° east of the start position. Absolute drift length since ridge formation date (Section 4.3) is 600 to 700 km leading to an average drift speed of 0.12 to 0.14 ms^{-1}.

4.3 Age of Ridges in 2013

Semi-empirical FDD models (Eq. 3 to Eq. 6) based on Stefan's analytical solution (Stefan, 1891) predict ice growth from air temperature alone. They are commonly used to model ice growth when detailed meteorological and oceanographic measurements are missing. The calculations were performed in two steps. First a possible ice formation date for the level ice was estimated. For this the

FDD's from the 29th of April backwards in time were used until the level ice thickness of 67 cm was reached. As a second step, the date when ice thickness reached the measured ice block thickness was calculated from the date of the initial ice growth obtained from step one. The time when the ice thickness equals the block thickness was assumed to be the date of ridge formation. Both ERA and NCEP data for temperatures along the respective drift track for the winter/spring season 2013 are given in Fig. 14. The NCEP data resulted in some colder temperature peaks from middle of February until middle of April but are overall in good agreement with the ERA data. Earlier work showed a good agreement for both data sets with actual field measurements during a two week field campaign in 2012, Petrich and Bonath (2014). The fluctuations of changes in the case of temperature and wind speed were in phase. However, the extreme values were not as pronounced as in the field data.

The results from ice growth calculations are shown in Fig. 16. Since the ERA-data gave milder temperatures during this period, the possible ice formation period for different FDD models was predicted earlier than for the NCEP data. The total interval of possible ice formation was from 23rd of February (Kovacs) to 10th of March (Anderson). Accordingly the possible ridge formation date, where the ice thickness equals the ice block thickness was between 2nd of March (Kovacs) and 14th of March (Anderson). This is a time period of 13 days. Assuming that the wind is a driving factor for ridge formation, the time period for possible ridge formation could be narrowed down to 10 days between 3rd and 12th of March. Wind speed peaks that are sufficiently high to ridge an ice cover of 0.26 m thickness (according to equations from Parmerter and Coon, 1973 and Leppäranta, 1981) occurred on 3rd (15.4 m/s), 5th (16.3m/s) and 9th of March (14.4m/s), see Fig. 15. As a result, the ridge R3-2013 was 7 to 8 weeks old at the time of field measurements.

5 Discussion

5.1 Ridge Profiles

Typical ridge dimensions have lately been presented by Strub-Klein and Sudom (2012) based on ridge data from over 300 first – year ridges. Table 6 shows how different ridge dimensions correlate to each other and compares the present data with the findings from Strub-Klein and Sudom (2012). The

maximum total ridge thickness (H_S+H_K) is close to what was found earlier in the Barents Sea, implying that the presented ridges were of medium size and comparable with other ridges in the Barents Sea. The keel to sail ratios (H_K/H_S) for the presented ridges are all below 3.9, and significantly lower than the average values for these regions, which are 5 for Svalbard and 4.4 for the Barents Sea. This is probably due to higher measured sail heights (2.3 in average) and lower keel depths (6.1 in average) than measured earlier in these areas (2.1 and 8.5 respectively for the Barents Sea). Suitable ridges were chosen as apparently biggest ridges within the area, where a high sail height was a decisive factor. R2-2012 is a good example showing that the drilling position for doing ridge measurement matters, because if only cross-section B would have been drilled, H_K/H_S would have resulted in 8.38 instead of 3.94. Correlations made with keel widths and sail widths (Table 5) are given for completeness but do generally show high variations. Different ridge shapes and occasional merging of the ridges with a rubble field, as it is the case for R2-2013, make comparisons difficult. The ridges investigated in this study had triangular sail shape as proposed by e.g. Timco and Burden (1997) with exception of R2-2013, where both drilled cross-sections showed trapezoidal ridge sails. The observed keel shapes in this study barely complied with the perfect triangular or trapezoidal keel shapes recommended both in literature (e.g. Kankaanpää, 1988; Timco and Burden, 1997, Strub-Klein and Sudom, 2012) and ISO 19906 (2010). Yet R1-2011 and R2-2012 are both symmetrical and approximately triangular in both keel and sail. Both ridges are straight along its spine instead for sinusoidal and differ from the other ridges in the way that R1-2011 is located in landfast ice and R2-2012 is built from thick ice. Some of the ridges with sinusoidal spines, e.g. the ridges from 2013 resemble the asymmetrical ridge profiles that were generated from ice tank tests by Tuhkuri and Lensu (2002). This gives evidence that the sinusoidal spines are a result of initial finger rafting before ridging.

Regarding the variations in keel shape, the keel area could provide better information on the keel size (Obert and Brown, 2011), rather than only considering ridge heights. Dalane et al. (2015) showed in a series of ice-tank measurements on ridge-structure interaction that forces from unmanaged ridges increased almost linearly with increased ridge cross-sectional area, giving that ridge parameter a major importance. The present ridge areas are listed in Table 2 for both, sail, keel and consolidated part.

Often was the area of the consolidated part greater than the keel rubble area. In average was the consolidated area 58% of the ridge keel, with a minimum value of 33% for R2-2013. Timco and Burden (1997) found a best-fit linear relation where the sail area is direct proportional to the keel area multiplied by a factor of 8. This factor is only valid for R2-2013 with a relatively large trapezoidal keel, but would greatly underestimate the keel areas for the other ridges. This is probably because both keel depth and keel width were bigger in relation to sail height than the average ratios from the ridges presented by Timco and Burden (1997). The average ratio A_K/A_S for the present study is 14 along the cross-sections and 3 along the spines. The difference can simply be explained by the fact that firstly the sail has its maximum values along the spines, but not necessarily the keels. Secondly the sail width perpendicular to the spine is much smaller than the keel width. In this study keel areas ranged from 52 to 518 m^2, whereof the highest values conform to areas along the spine. Obert and Brown (2011) presented 3197 keel areas recorded by sonar measurements whereof 60% of all ridge keels areas (ranging from 2.6 m^2 to 851 m^2) were smaller than 40 m^2. This is because all passing ice features were recorded and not only the apparently bigger ridges as it was done in this study. Obert and Brown (2011), who also presented load measurements of the ridges against a bridge peer, could not point out any direct connection between keel area and the magnitude of ice load. Therefore the consolidated area is probably more relevant, at least for the Bridge across the Northumberland Strait.

5.2 Macroporosity and consolidation

The calculated average sail macroporosity was 13% vs. the average keel macroporosity value of 23%, which are lower than most values presented in literature (Table 7) but in good agreement with the values presented by Ervik et al. (2018). Present results showed variation of the sail macroporosity between 0 and 30% and values from less than 1% up to 51% in the case of keels. If excluding sail porosities equal to zero (R1-2011, R2-2011 and partly R2-2012), with sail height close to block thickness, the average sail porosity is 19% and conforms to most data presented in literature. If further excluding the keel rubble porosities from R1-2011 and R1-2013, where a high amount of slush complicated the profile drilling, the average rubble porosity is with 30% in perfect agreement with earlier reported values. Porosity variations in the magnitude of up to 15% were found within the same

ridge for different profiles as in R2-2012 for ridge sails and in R2-2013 and R3-2013 for both keels and sails. Veitch et al. (1991) reported variations in the same order with ridge porosities ranging from 22% to 38% for different cross-sections of the same ridge. Ridge porosity values have commonly high variations between different literature sources probably caused by several uncertainty factors. For published porosity data it is often unclear whether keel porosity is related to only the unconsolidated keel rubble or the keel inclusive the consolidated layer, which can differ considerably, see Table 3. Further the usage of different measurement techniques to investigate the internal structure of a ridge matters, Strub-Klein and Sudom (2012). The biggest drawback of mechanical drilling is the purely sensuous and visual assessment of the drilling resistance and the material transported upwards with the drilling rod; the accuracy is especially low for soft and warm ice. In such case it is very difficult to distinguish between soft ice and slush. When the slush layer is on top of the ice, it gets virtually impossible to determine whether the material transported upwards from drilling is wet or dry. Thermal drilling is used e.g. by Kharitonov (2008, 2012) and Beketsky et al. (1996). The determination of the macroporosity maybe more accurate since ice consistency and pores are determined from the drill penetration rate, anyhow an element of uncertainty is the definition of critical penetration rates for distinguishing between hard and soft ice. Moreover in their studies only ice free zones are identified as pores, whereas for most studies done by mechanical drilling, very soft ice/slush are accounted for as pores. This might be one reason for the lower values presented by Kharitonov (2008, 2012). Variations in sail macro porosity for different ridges could be related to differences in the ratio of sail size vs. block thickness. Fig. 17 shows a tendency of increasing sail porosities for low ratios. One needs also consider that macro porosity is determined based on a limited number of drill holes, introducing statistical errors. Therefore Kankaanpää (1989) used the term apparent macro porosity. A matter for future studies could be if a large number of ideally uncorrelated measurements would be preferable. Dealing carefully with porosity data is a significant issue and needs more attention in future. Surkov (2001) studied the correctness of porosity data obtained from drill holes in laboratory experiments and found the real or volumetric macro porosity to be underestimated by 15 to 25 % by spot drillings.

Kharitonov (2012) and others reported that keel porosity increases with depth which could then slow down ridge consolidation. The porosity increases for all three ridges from 2013 (Fig. 18) until a certain

depth is reached, where only few boreholes still encounter ice. At this point porosity partly even turns zero, since only single ice blocks without gaps are drilled through. The non-zero start values at depth from 0 to -0.5 m of the three ridges depend on some slush-filled pools on the surface of the ridges which were accounted for as pores. The increase of porosity is not constant and ridges R2-2013 and R3-2013 show several local maxima and minima which could indicate a layered block structure in the ridge. This fluctuating porosity distribution at a certain depth is similar in the depth profile presented by Kharitonov (2012). Very high porosity values of 0.4 to 0.6 (maximum 0.7) appear commonly in the middle of the ridge keels. From a thermodynamic model, Høyland (2002) concluded rubble porosity to be the most important parameters influencing consolidation besides snow. Høyland (2002) derived a relationship between the consolidated layer and the level ice thickness from analytical solutions, depending on the ridge macro porosity:

$$H_{CL}^2(t) = H_{CL,0}^2 + \frac{H_{LI}^2(t) - H_{LI,0}^2}{\eta_M}, \qquad (7)$$

The application of Eq.7 to the measured values for R3-2013 with H_{LI}=0.67 m, $H_{LI,0}$=0.26 m and $H_{CL,0}$=0 would result in H_{CL}=0.86 m and thus underestimate the measured consolidated layer by factor 2.1. This is due to a high keel rubble porosity of 51%. Regarding the fact that porosity increases with depth and considering the amount of crushed ice found within the ridge from thin sections (Fig. 12), the keel porosity for the consolidated part before refreezing was probably much lower. Small crushed ice pieces and slush would float upwards and fill the gaps between bigger blocks shortly after the turbulences from ridge formation relaxed. Thus the thermodynamic consolidation rate for the upper part could be underestimated when constant macro porosity is assumed throughout the keel depth. The measured average consolidated layer thickness of 1.8 m for R3-2013 (Table 4) would be obtained from η_M equal to 10%. Fig.18 shows that the measured macroporosity was in fact lower than 40% in the upper 2 m of the keel. It has also to be kept in mind that Eq.7 only applies for the main phase of consolidation. The initial consolidation, subjected to the internal re-distribution of energy between cold ice and the surrounding warmer water until a smooth temperature distribution appears, may lead to a higher consolidation rate than calculated with Eq.7.

The average consolidated layer thickness in the Barents Sea and Svalbard regions presented by Strub-Klein and Sudom (2012), which are 1.55 m and 1.37 m respectively are exceeded by the ridges studied here, where the consolidated layer in average was 1.74 m (Table 4). The consolidated layer presented by Strub-Klein and Sudom (2012) only considers the part below water line, which would result in averaged 12% lower values for the recent study and thus in conformity with the literature. The average maximum thickness of consolidation for all ridges was 4 m, which was twice the value found by Strub-Klein and Sudom (2012). It is suggested in ISO 19906 (2010) that the consolidated layer thickness can be assumed to be two times the level ice thickness. The attempt to relate the level ice thickness to the consolidated layer thickness has practical reasons since level ice thickness is more easily accessible. But for field data it is not always clear whether the surrounding level ice is the same as from which the ridge originated. This is the case for the ridges R2-2012, R1-2013 and R3-2013 as extracted from ice texture studies, for the other ridges it can only be assumed. The ridges investigated here have in eight out of eleven cases ratios of H_{CL}/H_{LI} between 2 and 3, when using the average thickness for consolidation. Both Kharitonov (2008) and Høyland (2007) report lower ratios, ranging from 0.83 to 1.63 and from 1 to 1.7 respectively. The ice growth is changing seasonally and therefore can the age and formation date of the ridges be highly influencing factors causing the differences.

Timco and Burden (1997) show that a high variability is always present for the consolidated layer thickness and gave a measure for it as presented in Table 8. The smallest variability, presented by Høyland (2002), may depend on the ridge origin, which is landfast ice in only that case. Even though variations were higher for the present ridges with a factor of 11.6 for variability, the highest factor with 20.0 for variations was obtained by Strub-Klein and Sudom (2012). For the present data the mean of the minimum to average thickness values is very low, due to values equal to zero coming from slush pools just around water level. Neglecting these slush pools would not correctly follow the present definition of the consolidated layer anymore and is therefore not done, but more realistic values for a consolidated layer could be expected and a lowering of the variability factor C_{Max}/C_{Min}.

Its variability is a challenge for estimating a representative consolidated layer thickness. Similar to the determination of the porosity is also the determination of the consolidated layer sensitive to the

measurement method. Depending on the method, different factors are defining the consolidated layer. Thermal methods, such as temperature measurements on ice cores or with thermistor-strings would define the lower border of the consolidated layer where measured temperatures reach freezing temperature. Mechanical methods such as drilling or compressive strength tests define the consolidated layer by ice strength or consistency. The lack of the definition of the consolidated layer and of a standardized measurement technique can explain the variability of the data presented by Strub-Klein and Sudom (2012). Høyland (2007) pointed out that temperature profiles result in lower values for the consolidated layer thickness than mechanical drilling. From the temperature profiles in Fig. 10 it is obvious that the measured ice temperatures at the respective lower boundary for consolidation are lower than the freezing temperatures for all three ridges. According to the temperature profiles h_{CL} would be 2.1 m instead of 0.5 m for R1-2013 at B6, at least 1.4 m instead of 0.3 m for R2-2013 at B5 and at least 2.0 m instead of 1.4 m for R3-2013 at B15. This is contradictory to Høyland (2007). Obviously high saline interstitial water was detected by drilling, maybe pockets of frazil/crushed ice built under ridge formation, located such as to inhibit efficient drainage. Expelled brine concentrates within the gaps so that very high bulk salinity prevents development of strength during consolidation even at -5 C. Høyland and Løset (1999) treated those gaps as brine pockets and considered them as macro pores within the consolidated layer.

R2-2011 has two unreasonable high peaks for consolidated layer thickness, which can either be referred to as measurement errors by missing gaps or accidently ice blocks were lying on top of each other, connected by freeze-bonds. It was noticed during field work, that the ridge sail consisted of big vertical blocks (Fig. 4a). If the same phenomena occurred in the keel, the high consolidated layer values could be explained by drilling through vertical blocks. Leppäranta and Hakkala (1992) refer to the uneven void distribution within ridges.

5.3 Ice block dimensions

Tucker et al. (1984) found up to three different ice block thicknesses within a ridge sail. In the present study only one predominant peak for each ridge was found, i.e. the modal block thickness. 80% (and for R3-2013 even 90%) of all measured ice blocks deviated less than 0.1 m from the accordingly

modal block thickness. Shafrova and Høyland (2008) reported higher variations for ice block thickness, but their field measurements were performed later in the season which could have caused higher degree of aging of ice blocks, by e.g. erosion due to wind and solar radiation (Strub-Klein and Høyland, 2011). Thickness variations in ice blocks can also come from natural ice growth variations in ice floes initiated by uneven snow cover, or cracks. Field observations have shown that snow ice has built on top and between ice blocks, probably formed from flushing during ridge building or snow-ice formation through snow-metamorphism (Leppäranta, 1983). The mono-modal block thickness distribution for the present ridges indicates that they either formed from two floes with equal thicknesses or that only one of the floes broke during ridge formation. Both cases maybe applicable: Ridges R2-2012 and R2-2013 had level ice on one side and a thick rafted ice or rubble field on the other side, i.e. presumed that only the thin level ice failed, while ridges R1-2011 and R1-2013 had equal level ice thickness on either side of the ridge.

Ice block thickness is often related to the sail height. For example Parmerter and Coon (1972) identified ice block thickness as a limiting factor for maximum sail height. Hopkins (1998) suggested that this limit appears to be rarely met in arctic ridges. Tucker and Govoni (1981) related the sail height to the square root of ice block thickness multiplied by a factor of 3.69 with a best-fit curve of field data. The factor was recently updated to 3.73 by Strub-Klein and Sudom (2012). Ridges R1-2013 and R2-2013 comply with the curve, whereas R2-2012 is significantly below the curve, meaning that low driving forces accompanied the ridging event. High driving forces for the ridging event are R3-2013 are accepted since maximum sail height exceeded even the value obtained from the empirical upper limit expression by Tucker and Govoni (1981). It can be concluded that the magnitude of driving forces for ridging differs certainly significantly for different events, so that one can argue if the block thickness can really directly be related to sail height. Only very few ridges develop sufficiently high driving forces to enabling to reach a limiting maximum sail height as stated by Hopkins (1998).

Parmerter and Coon (1972), Hopkins (1998) and Tuhkuri and Lensu (2002) described that ridge growth tends to continue in lateral direction when driving forces for vertical formation becomes insufficient. Tucker et al. (1984) found a strong relationship $W_S = 16.35\sqrt{h_{bl}}$ between the sail width

W_S and the ice block thickness h_{bl}, which is only valid in the absence of lateral ridge growth. This formula fits R3-2013 very well, but overestimates the width for the narrow sails of R1-2013 and R2-2012. Yet the deviations are within 3m and approximately in line with the formula, thus can be a result of the subjective assessment of the sail width determination. The width of the trapezoidal sail from R2-2013 is underestimated by 6m. This fact and the trapezoidal sail shape could be a result of lateral growth of the ridge sail.

Surface shapes from ice blocks are in most cases not perfectly rectangular, yet the surface area was defined as the product of d_1 and d_2 (Section 2.2). The correlation described by Tucker et al. (1984) that the largest block surface areas belong to the thickest blocks can be confirmed (Table 3), as the blocks with highest block thickness also had in average the biggest block areas.

The ratio d_2/d_1 characterizes ice block shape. The closer this shape parameter is to 1, the more quadratic the ice blocks can be expected. Round ice blocks were barely observed during the field studies. Results show that 80 % of all ice blocks had a shape parameter between 1.0 and 2.0, Fig. 19, which is in accordance with data presented by Sayed and Frederking (1989) and Surkov and Truskov (2003). A 3-parameter lognormal distribution was suggested as best-fit to three data sets, Fig. 20. One should be aware of that this fit is purely empirical and allows the data to be slightly below 1. The shape parameter was in average 1.5, which is similar to Høyland (2007), Kankaanpää (1989) and Veitch et al (1991) who all found average shape parameters between 1.5 and 1.6. Since the block shape parameter is noticeable similar for all block measurements presented in literature, it could be worthwhile to further study if the shape parameter indicates any prevailing failure mechanism, even though a variation of different failure modes of the ice floe during a ridging event should be expected.

When comparing the block shape with ice block thicknesses for each single ice block, it appears as though the likelihood of encountering elongated blocks (i.e. high d_2/d_1) decreases with increasing block thickness, Fig. 21. Yet a regression analysis giving a p-value of 0.19 rejects the hypothesis of any significant relationship between the variables h_{bl} and the ratio d_2/d_1, meaning that the block shape is independent of ice block thickness. Kulyakhtin (2014) proposed that the ratio between the longest axis d_2 and the block thickness has a unique distribution for each ridge. Confirmation with the present

data is given with Fig. 22, which further shows that the distributions assimilate the higher number of measured ice blocks involved. Comparing the present data to ice block data from literature, Fig.23, one distinct distribution followed by all data sets can doubtless be identified. The ratio d_2/h_{bl} is following clearly a log-normal distribution (Fig. 24) suggesting mean value and standard deviation to be equal to 1.22 and 0.46 respectively.

Ice block inclination was estimated with respect to the horizontal plane. The maximum inclination between block and horizontal plane was 50° in the case of ice blocks thicker than 0.60 m. The average angle for ice blocks between 0.60 m and 1 m thick was 14°, similar to results presented by Kankaanpää (1989). For ice thinner than 0.60 m instead the average inclination was much higher with 50°, which complies with the results of Shafrova and Høyland (2008) for ridges located east of Svalbard. Ice block thickness seems to affect the inclination angle. The average inclination for all ice blocks studied in the present research was 48° (average h_{bl}=0.36) which is higher than the inclination angles of all ice blocks studied by Høyland (2007) with average inclinations of 39° (average h_{bl}=0.38). Measurement errors can be expected from the present study due to the rough estimate of inclination angles.

5.4 Ridge formation

The method to reconnoiter ridge formation from the ridge internal structure has been used earlier by Tuhkuri et al. (1999) and Kankaanpää (1997). Tuhkuri et al. (1999) cut a profile of thick sections through the ridge sail and the consolidated part with a chain saw to study the ice block configuration in the ridge. Kankaanpää (1997) took spot samples of the studied ridge cross-sections and could identify rafting as a part of the ridging process through ice texture analysis.

The ridging scenario described in Fig. 12a and Fig. 12b complies with the ridging scenarios described in literature. Tuhkuri and Lensu (2002) obtained from laboratory tests that initially rafting of the thinner ice sheets is followed by ridging. Multiple rafting, as it was observed here with several ice layers rafted upon each other, has been observed the ridges studied by Kankaanpää (1997) and Tuhkuri et al. (1999). The rafting scenario described by Tuhkuri et al. (1999) equals the rafting scenario here, where the left thick ice sheet is overthrusted by long multiple layers of thin rafted ice

sheets. The difference is that at least 10 rafted layers (compared to 5) where observed in this study built up of 2 to 6 cm thin ice layers (compared to 8 cm). As described in Kankaanpää (1997) very thin lead ice (from 3cm) is strong enough, but also flexible enough to undergo bending and rafting without breakage. The lead ice in this study probably formed shortly before the ridging event and has not undergone any surface wrinkling that would increase frictional forces during rafting. Rafting of one layer will possibly end when the bending forces exerted by the overriding of the thick ice sheet exceed the tensile strength of the lead ice. At some point the rafting would turn into ridging. As the ridge R3-2013 was built up of ice blocks from the adjacent level ice sheet, ridging continued after the thin lead ice depleted. The scenario that ridging continuous with the adjacent thicker ice sheet after rafting and ridging of lead ice when driving forces are sufficiently high, was earlier described by Weeks et al. (1971) and Tucker et al. (1984). From section 5.3, high driving forces can be assumed for this ridging event. It is not sure when the changeover from lead ice to level ice occurred in this ridging scenario. Since no ice blocks with lead ice thickness were found, it is not impossible that the lead ice was only rafting and the ridging continued instead with the 0.26 m level ice floe. But the fact that a big amount of small crushed ice was found within the ridge keel could be a result of crushing and compression of thinner, weaker lead ice in between two thicker ice floes.

A time span of 10 days for possible ridge formation date was found, when taken into account the slight differences from the data sets for weather and the different FDD models. Several wind peaks during that period could have initiated ridge building. The ridge age at time of investigation was 7 to 8 weeks which could conform to the degree of consolidation and the observed deterioration of the sail rubble.

The ridge origin was backtracked by free-drift approximation and results in a location east of Svalbard. When comparing the estimated drift path with drift trajectories generated by IFREMER for different dates, the drift directions correlate to the drift trajectories. The applied free-drift assumption, which was valid for surface winds, requires close drift ice fields and drift passage free from distortions caused by shorelines or shallow waters. Both requirements were met during the time from ice formation until the ridges end position. One could argue that ice deformation such as ridging should be accompanied by large internal stresses and consequently makes free-drift approximation less

applicable. Considering that the ice cover was broken and the ice floe that formed the ridge was generally thin (0.26 m during ridge formation and 0.67 m during field measurements), the effect of internal ice stresses should be negligible.

The presented attempt of retracing the ridging event for the investigated ice ridge is accompanied by uncertainties, but still holds a number of matches with actual measured data. Conformity of results was found for free drift and for theoretical ridging process with actual ridge structure. A first attempt to relate ridge ice properties to environmental conditions from large-scale products was earlier presented by Petrich and Bonath (2014) and applied to ridge R2-2012 and good agreements between models and physical values were found. A detailed study on the microstructure and physical parameters of pressure ridges could generally give more information than what is extracted from field studies so far.

6 Conclusions

This paper contributes to a better understanding of ice ridges. Large scatters for ridge geometry data is a persistent problem that has to be dealt with. Ice ridges do not build under equal conditions and are exposed to different natural occurrences. The morphological data from a comprehensive field study comprising the measurements of 6 pressure ridges were presented with the aim to provide complete data for further research and attention was paid to so far poorly reported data. The knowledge gaps on ice ridge data identified by Strub-Klein and Sudom (2012) such as ridge cross-sectional areas, ridge consolidation and block dimensions were covered. For the first time profiles of ridges along and across the ridge spine were presented. The data were analyzed with regard to previous publications and new approaches to analyze and evaluate ridge data were suggested. Overall ridge data would be easier to compare if there would be general agreements on the definition of important ridge parameters such as the consolidated layer and ridge porosity. The main findings from the recent study are summarized as follows:

- The determination of ridge cross-sectional areas, for sail, keel and the consolidated layer is rarely reported, but an effective way to approximate the overall magnitude of ice ridges, not

least due to the variability of ridge keel shapes. The keel area to sail area ratio was 14 for the sections perpendicular to the spine and 3 for the measured sections along the ridge spine. Furthermore the ratio of consolidated ice area to ridge keel area can be tremendous within a cross-section. The consolidated area always exceeded 33 % and was in average 58% of the ridge keel area.

- The consolidated layer thickness was in average from 1.0 m to 2.8 m, and this is higher than many other have reported and what models predict. The ratio of consolidated layer and level ice thickness ranged from 1.4 to 3 and was between 2 and 3 for 8 of 11 cross-sections, based on the assumption that the surrounding level ice has the same origin as the ice that formed the ridge.
- Macroporosity within the ridge keel is highly variable with depth. After a fast increase in the upper keel part follows a fluctuating porosity distribution where macroporosity values can be as high as 70%. Macroporosity approaches zero quickly in the lowest keel part, where the ridge keel only consists of some single, underlying ice blocks.
- Even though the absolute values for ice block dimensions differ for different ridges, the distributions of the ratio between the longest and shortest axis of ice blocks and the ratio between the longest axes and the block thickness are similar for all ridges. The ratio d_2/d_1, describing roughly the block surface shape, is in average 1.5 and follows a unique trend which can be described by a 3-parameter lognormal distribution. The ratio d_2/h_{bl} is lognormal distributed with $\mu = 1.22$ and $\sigma=0.46$. Hence the distribution of ice block sizes and block shapes within a ridge is predictable and ice blocks for a ridge can be determined from the block thickness.

The re-creation of a possible ridge formation scenario was attempted for R3—2013. It is possible to identify the process of ridge formation based on information on ridge morphology and ice texture with reasonable results. A realistic ridge history can be recreated from ice growth models, reanalyzed weather data and reconstruction of ice drift path. The accuracy of possible formation date lies within a

time span of two weeks. The identification of ridge age and ridge origin is one step forward to determine the growth rate of the consolidated layer.

Acknowledgements

This work was supported by the Research Council of Norway project number 195153. CP would like to acknowledge support of the Research Council of Norway PETROMAKS2 program, project 243812 (MOSIDEO). The Coldtech group attending the field work and the Crew on KV Svalbard are thanked for their support. Two anonymous reviewers and the editor Jukka Tuhkuri are thanked for their help to improve the manuscript. ERA Interim reanalysis data were provided by European Centre for Medium-Range Weather Forecasts (ECMWF), from their Web site at http://www.ecmwf.int/en/research/climate-reanalysis/. NCEP Reanalysis data were provided by the NOAA/OAR/ESRL PSD, Boulder, Colorado, USA, from their Web site at https://www.esrl.noaa.gov/psd/. Ice drift information was provided by CERSAT/IFREMER.

References

Amundrud, T. L., Melling, H., Ingram, R.G. & Allen, S.E., 2006. The effect of structural porosity on the ablation of sea ice ridges. Journal of Geophysical Research: Oceans 111 (C6). http://dx.doi.org/10.1029/2005JC002895.

Anderson, D. L., 1961. Growth rate of sea ice. Journal of Glaciology 3 (30), 1170-1172. Retrieved from http://authors.library.caltech.edu/45124/1/Anderson_1961p1170.pdf

Beketsky, S. P., Astafiev, V.N. & Truskov, P.A., 1996. Structure of Hummocks Offshore of Northern Sakhalin. Proceedings of the 6th lnternatiol Offshore and Polar Engineering Conference 1996. Los Angeles,USA. Vol 2, 398-400. Retrieved from https://www.onepetro.org/download/conference-paper/ISOPE-I-96-144?id=conference-paper%2FISOPE-I-96-144

Bonath, V., Edeskär, T., Lintzén, N., Fransson, F. & Cwirzen, A., (in Review). Properties of ice from first-year ridges in the Barents Sea and Fram Strait.

Colony, R., Thorndike, A. S., 1980. The horizontal coherency of the motion of summer arctic sea ice. Journal of Physical Oceanography 10 (8), 1281 – 1289. http://dx.doi.org/10.1175/1520-0485(1980)010<1281:THCOTM>2.0.CO;2

Comfort, G., Singh, S. & Dinovitzer, A., 1998. Limit-force ice loads and their significance to offshore structures in the Beaufort Sea. International Journal of Offshore and Polar Engineering 8(01).

Dalane, O., Aksnes, V. & Løset, S., 2015. A Moored Arctic Floater in First-Year Sea Ice Ridges. Journal of Offshore Mechanics and Arctic Engineering 137 (1), 011501-011501-8. http://dx.doi.org/10.1115/1.4028814

Dee, D. P., Uppala, S., Simmons, A., Berrisford, P., Poli, P., Kobayashi, S., Andrae, U., Balmaseda, M., Balsamo, G., Bauer, P., Bechtold, P., Beljaars, A., van de Berg, L., Bidlot, J., Bormann, N., Delsol, C., Dragani, R., Fuentes, M., Geer, A., Haimberger, L., Healy, S., Hersbach, H., Hólm, E., Isaksen, L., Kållberg, P., Köhler, M., Matricardi, M., McNally, A., Monge-Sanz, B., Morcrette, J., Park, B., Peubey, C., de Rosnay, P., Tavolato, C., Thépaut, J. & Vitart, F., 2011. The ERA-Interim reanalysis: configuration and performance of the data assimilation system. Quarterly Journal of the Royal Meteorological Society, 137(656), 553–597. http://dx.doi.org/10.1002/qj.828

Ervik, Å., Høyland, K. V., Shestov, A. & Nord, T. S., 2018. On the decay of first-year ice ridges: Measurements and evolution of rubble macroporosity, ridge drilling resistance and consolidated layer strength. Cold Regions Science and Technology, 151, 196-207. http://dx.doi.org/10.1016/j.coldregions.2018.03.024

Hopkins, M. A., 1994. On the ridging of intact lead ice. Journal of Geophysical Research: Oceans 99(C8), 16351-16360. http://dx.doi.org/10.1029/94JC00996

Hopkins, M. A., 1998. Four stages of pressure ridging. Journal of Geophysical Research: Oceans 103(C10), 21883-21891. http://dx.doi.org/10.1029/98JC01257

Hopkins, M.A., Hibler, W.D., 1991. On the shear strength of geophysical scale ice rubble. Cold Regions Science and Technology 19 (2), 201-212. http://dx.doi.org/10.1016/0165-232X(91)90009-6.

Hopkins, M. A., Hibler, W.D. & Flato, G.M., 1991. On the numerical simulation of the sea ice ridging process. Journal of Geophysical Research: Oceans 96(C3), 4809-4820. http://dx.doi.org/10.1029/90JC02375

Høyland, K. V., 2002. Simulations of the consolidation process in first-year sea ice ridges. Cold Regions Science and Technology 34(3), 143-158. http://dx.doi.org/10.1016/S0165-232X(02)00002-2

Høyland, K. V., 2007. Morphology and small-scale strength of ridges in the north-western Barents Sea. Cold Regions Science and Technology 48(3), 169-187. http://dx.doi.org/10.1016/j.coldregions.2007.01.006

Høyland, K. V., Løset, S., 1999. Measurements of temperature distribution, consolidation and morphology of a first-year sea ice ridge. Cold Regions Science and Technology, 29(1), 59-74. http://dx.doi.org/10.1016/S0165-232X(99)00004-X

ISO19906, 2010. Petroleum and Natural Gas Industries—Arctic Offshore Structures (2010)

Kalnay, E., Kanamitsu, M., Kistler, R., Collins, W., Deaven, D., Gandin, L., Iredell, M., Saha, S., White, G., Woollen, J., Zhu, Y., Chelliah, M., Ebisuzaki, W., Higgins, W., Janowiak, J., Mo, K.C., Ropelewski, C., Wang, J., Leetmaa, A., Reynolds, R., Jenne, R. & Joseph, D., 1996. The NCEP/NCAR 40-Year Reanalysis Project. Bulletin of the American Meteorological Society, 77(3), 437-472. http://dx.doi.org/10.1175/1520- 0477(1996)077<0437:TNYRP>2.0.CO;2

Kankaanpää, P., 1988. Morphology of a Baltic Sea ice pressure ridge. Geophysica 24(1-2), 15-33. Retrieved from http://www.geophysica.fi/pdf/geophysica_1988_24_1-2_015_kankaanpaa.pdf

Kankaanpää, P., 1989. Structure of first year pressure ridges in the Baltic Sea. Proceedings of the 10th International Conference on Port and Ocean Engineering under Arctic Conditions (POAC) 1989. Luleå, Sweden. Vol. 1, 87-102. Retrieved from http://www.poac.com/PapersOnline.html

Kankaanpää, P., 1997. Distribution, morphology and structure of sea ice pressure ridges in the Baltic Sea. Fennia - International Journal of Geography 175(2), 139-240.Retrieved from https://fennia.journal.fi/article/view/8919

Kharitonov, V. V., 2008. Internal structure of ice ridges and stamukhas based on thermal drilling data. Cold Regions Science and Technology 52(3), 302-325. http://dx.doi.org/10.1016/j.coldregions.2007.04.020

Kharitonov, V. V., 2012. Internal structure and porosity of ice ridges investigated at «North Pole-38» drifting station. Cold Regions Science and Technology 82, 144-152. http://dx.doi.org/10.1016/j.coldregions.2012.05.018

Kovacs, A., 1996. Sea Ice: Part II. Estimating the Full-Scale Tensile, Flexural, and Compressive Strength of First-Year Ice. CRREL Technical Report 96-11. CRREL, Hanover, NH. Retrieved from http://www.dtic.mil/get-tr-doc/pdf?AD=ADA317247

Kulyakhtin, S., 2014. Distribution of ice block sizes in sails of pressure ice ridges. Proceedings of the 22nd IAHR International Symposium on Ice 2014. NEWRI, Nanyang Technological University, Singapore, pp. 235-240.

Leppäranta, M., 1981. On the structures and mechanics of pack ice in the Bothnian Bay. Finnish Marine Research, 248, 3–86. Retrieved from http://hdl.handle.net/10138/169141.

Leppäranta, M., 1983. A growth model for black ice, snow ice and snow thickness in subarctic basins. Hydrology Research 14 (2) 59-70.

Leppäranta, M., 2011. The drift of Sea Ice. Springer-Verlag (2011). http://dx.doi.org/ 10.1007/978-3-642-04683-4

Leppäranta, M., Hakala, R., 1992. The structure and strength of first-year ice ridges in the Baltic Sea. Cold Regions Science and Technology 20(3), 295-311. http://dx.doi.org/10.1016/0165-232X(92)90036-T

Leppäranta, M., Lensu, M., Kosloff, P. & Veitch, B., 1995. The life story of a first-year sea ice ridge. Cold Regions Science and Technology 23(3), 279-290. http://dx.doi.org/10.1016/0165-232X(94)00019-T

Nikitin, V., Kolesov, S., 1993. Stresses and forces under ice compacting. International Journal of Offshore and Polar Engineering 3(02).

Obert, K. M., Brown, T.G., 2011. Ice ridge keel characteristics and distribution in the Northumberland Strait. Cold Regions Science and Technology 66(2-3), 53-64. http://dx.doi.org/0.1016/j.coldregions.2011.01.004

Parmerter, R. R., Coon, M. D., 1972. Model of pressure ridge formation in sea ice. Journal of Geophysical Research, 77(33), 6565-6575. http://dx.doi.org/10.1029/JC077i033p06565

Parmerter, R.R. &Coon M. D. (1973). Mechanical models of ridging in the Arctic Sea ice cover. Aidjex Bulletin 19,59–112.

Petrich, C., Bonath, V., 2014. Relating sea ice drift to ice properties in Fram Strait. Proceedings of the 22nd IAHR International Symposium on Ice 2014. NEWRI, Nanyang Technological University, Singapore, pp. 751-758. Retrieved from http://www.diva-portal.org/smash/get/diva2:1013095/FULLTEXT01.pdf

Petrich, C., Eicken, H., 2010. Growth, Structure and Properties of Sea Ice. In Sea Ice, Second Edition (eds D. N. Thomas and G. S. Dieckmann), Wiley-Blackwell, Oxford, UK, 23-77. http://dx.doi.org/10.1002/9781444317145.ch2

Richter-Menge, J.A., Cox, G.F.N., 1985. A preliminary examination of the effect of structure on the compressive strength of ice samples from multi-year pressure ridges. Journal of Energy Resources Technology, 107(1), 99-102. Retrieved from https://energyresources.asmedigitalcollection.asme.org/pdfaccess.ashx?url=/data/journals/jertd2/26403/99_1.pdf

Richter-Menge, J. A., Elder, B. C., 1998. Characteristics of pack ice stress in the Alaskan Beaufort Sea. Journal of Geophysical Research: Oceans 103(C10), 21817-21829. http://dx.doi.org/10.1029/98JC01261

Sand, B., Bonath, V., Sudom, D. & Petrich, C., 2015. Three years of measurements of first year ridges in the Barents Sea and Fram Strait. Proceedings of the 23rd International Conference on Port and Ocean Engineering under Arctic Conditions (POAC) 2015. Trondheim, Norge. Retrieved from http://www.poac.com/Papers/2015/pdf/poac15Final00033.pdf

Sayed, M., Frederking, R.M.W, 1989. Measurements of ridge sails in the Beaufort Sea. Canadian Journal of Civil Engineering 16(1), 16-21. http://dx.doi.org/ 10.1139/l89-003

Shafrova, S., Høyland, K. V., 2008. Morphology and 2D spatial strength distribution in two arctic first-year sea ice ridges. Cold Regions Science and Technology, 51(1), 38-55. http://dx.doi.org/10.1016/j.coldregions.2007.05.011

Smith, L. C., Stephenson, S. R., 2013. New Trans-Arctic shipping routes navigable by midcentury. Proceedings of the National Academy of Sciences, 110(13), E1191-E1195. Retrieved from http://www.pnas.org/content/pnas/110/13/E1191/1.full.pdf

Stefan, J., 1891. Über die Theorie der Eisbildung, insbesondere über die Eisbildung im Polarmeere. Annalen der Physik, 278(2), 269-286. http://dx.doi.org/10.1002/andp.18912780206

Strub-Klein, L., Høyland, K. V., 2011. One season of a first-year sea ice ridge investigations. Winter 2009. Proceedings of the 21st International Conference on Port and Ocean Engineering under Arctic Conditions (POAC) 2011. Montreal, Canada. Paper No. POAC11-043. Retrieved from http://www.poac.com/PapersOnline.html

Strub-Klein, L., Sudom, D., 2012. A comprehensive analysis of the morphology of first-year sea ice ridges. Cold Regions Science and Technology 82(0), 94-109. http://dx.doi.org/10.1016/j.coldregions.2012.05.014

Surkov, G.A., 2001. Scientific and methodological principles of calculation for loads caused by ice ridges upon offshore oil and gas field facilities. Thesis of D.SC., Moscow (2001), 370.

Surkov, G.A., Truskov, P.A., 2003. Parameters of hummock-forming blocks of ice. Proceedings of the 17th International Conference on Port and Ocean Engineering under Arctic Conditions (POAC) 2003. Trondheim, Norway. Vol. 2, 87-102. Retrieved from http://www.poac.com/Papers/POAC03_V2.zip

Timco, G.W, Burden, R.P., 1997. An analysis of the shape of sea ice ridges. Cold Regions Science and Technology 25(1), 65-77. http://dx.doi.org/10.1016/S0165-232X(96)00017-1

Tucker III, W. B., Govoni, J.W., 1981. Morphological investigations of first-year sea ice pressure ridge sails. Cold Regions Science and Technology 5(1), 1-12. http://dx.doi.org/10.1016/0165-232X(81)90036-7

Tucker III, W. B., Sodhi, D.S., & Govoni, J.W., 1984. Structure of first-year pressure ridge sails in the Prudhoe Bay region. The Alaskan Beaufort Sea: Ecosystems and Environments, 115-135.

Tuhkuri, J., Lensu, M., 2002. Laboratory tests on ridging and rafting of ice sheets. Journal of Geophysical Research: Oceans. 107 (C9). http://dx.doi.org/10.10.1029/2001JC000848

Tuhkuri, J., Polojärvi, 2005. Effect of particle shape in 2D ridge keel deformation simulations. Proceedings of the 18th International Conference on Port and Ocean Engineering under Arctic Conditions (POAC) 2005. Potsdam, USA. Vol. 2, 939-948. Retrieved from http://ww.poac.com/Papers/POAC05_V2.zip

Tuhkuri, J., Lensu, M., & Saarinen, S., 1999. Laboratory and field studies on the mechanics of ice ridge formation. Proceedings of the 15th International Conference on Port and Ocean Engineering under Arctic Conditions (POAC) 1999. Espoo, Finland. Vol. 3, 1118-1129. Retrieved from http://www.poac.com/Papers/POAC99_V3_all.pdf

Veitch, B., Lensu, M., Riska, K., Kosloff, P., Keiley, P., & Kujala, P., 1991. Field observations of ridges in the Northern Baltic Sea. Proceedings of the 11th International Conference on Port and

Ocean Engineering under Arctic Conditions (POAC) 1991. St. John's, Canada. Vol. 1, 381-400. Retrieved from http://www.poac.com/Papers/POAC91_V1_all.pdf

Weeks, W.F., Kovacs, A., & Hibler, W.D., 1971. Pressure ridge characteristics in the arctic coastal environment. Proceedings of the 1st International Conference on Port and Ocean Engineering under Arctic Conditions (POAC) 1991. Trondheim, Norway. Vol. 1, 152-183. Retrieved from http://www.poac.com/Papers/POAC71_V1.zip

Zubov, N. N., 1945. L'dy Arktiki (Arctic ice). Izdatel'stvo Glavsevmorputi, Moscow.

Tables

Table 1. Coordinates for the six ridges studied from 2011 to 2013 (Sand et al., 2015)

Ridge:	Date:	Coordinates:
R1-2011	19 Mar	14.237 E, 79.847 N
R2-2011	29 Mar	22.521 E, 76.249 N
R2-2012	14 Mar	1.48 W, 79.93 N
R1-2013	27 Apr	26.645 E, 78.124 N
R2-2013	28 Apr	26.523 E, 78.116 N
R3-2013	29 Apr	26.381 E, 78.142 N

Table 2. Summary of measured geometric ridge data, including sail height (H_S), keel depth (H_K), sail and keel width (W_S, W_K), ridge length (L_R), sail and keel slope angles (α_S, α_K) and ridge areas for ridge sail (A_S), keel (A_K), the consolidated part (A_{CL}) and the total ridge (A_{Tot}). Profiles named 'A' were measured along the ridge spine, whereas the others were across.

	2011		R2-2012			R1-2013		R2-2013			R3-2013	
Profile	R1	R2	A	B	C	A	B	A	B	C	A	B
H_S (m)	2.0	2.4	1.7	0.8	1.4	2.0	1.8	2.0	2.0	2.1	3.3	2.7
H_K (m)	5.1	6.9	4.3	6.7	4.3	3.4	2.3	6.1	6.3	6.8	6.2	7.6
W_S (m)	8	9	-	9	8	-	14	-	12	12	-	10
W_K (m)	44	32	-	20	20	-	32	-	32**	32**	-	64
L_R (m)*	-	-	25	-	-	100	-	65	-	-	>120	-
α_S (°)	26	23	-	10	19	-	22	-	24	-	-	32
α_K (°)	12	20	-	28	19	-	8	-	11	15	-	10
A_S (m^2)	5	8	36	3	3	68	7	97	13	17	191	12
A_K (m^2)	82	114	97	63	36	222	52	278	139	135	518	281
A_{CL} (m^2)	-	66	84	41	36	130	33	120	63	45	224	126
A_{Tot} (m^2)	87	122	133	66	39	290	59	375	152	152	709	293

*L_R is the length of the ridge sail along the spine **The keel merges with a rubble field

Table 3. Macroporosity (μ_M) values for ridge sails and keels and the number of involved drill holes (n_{Sail} and n_{Keel}) for determining sail and keel porosities. Profiles named 'A' were measured along the ridge spine, whereas the others were across.

Macroporosity μ_M (%)												
	2011		R2-2012			R1-2013		R2-2013			R3-2013	
	R1*	R2*	A	B*	C*	A	B	A	B	C	A	B

Sail	0	0	6	0	0	16	12	19	15	26	26	30
Keel rubble	1**	31	22	20	27	1	<1	34	31	19	38	51
Keel(incl. CL)	1**	14	6	8	2	1	<1	21	17	13	23	33
n_{Sail} (-)	5	5	6	7	5	19	8	12	7	7	13	6
n_{Keel} (-)	23	15	6	11	11	19	17	12	17	17	13	27

*Sails consist of only few ice blocks and with snow/slush on top **Voids in the keel were not or hardly measurable

Table 4. The average consolidated layer thickness ($H_{CL,ave}$) and standard variations ($H_{CL,stdev}$), the minimum ($H_{CL,min}$) and maximum ($H_{CL,max}$) measured consolidated layer thickness and the number of boreholes n for the investigated ridge profiles. Profiles named 'A' were measured along the ridge spine, whereas the others were across.

	2011	R2-2012			R1-2013		R2-2013			R3-2013	
	R2	A	B	C	A	B	A	B	C	A	B
$H_{CL,\ ave}$ (m)	2.02	2.82	1.84	1.64	1.36	0.97	1.84	1.85	1.33	1.73	1.92
$H_{CL,\ stdev}$ (m)	2.00	1.16	0.97	1.13	1.11	0.53	1.07	1.13	0.78	1.29	0.57
$H_{CL,\ min}$ (m)	0.46	1.40	0.48	0.38	0	0.03	0.2	0.35	0.60	0	0.24
$H_{CL,\ max}$ (m)	6.27	4.15	3.90	4.15	3.20	2.40	3.97	3.20	3.52	4.43	2.93
n (-)	15	6	11	11	19	17	13	17	17	13	27
$H_{CL,ave}/H_{LI}$ (-)	2.53	3.00	1.96	1.44	2.12	1.50	2.97	3.00	2.15	2.58	2.87

Table 5. Summary of ice block dimensions (h_{bl}, d_1, d_2) and orientation (α_{bl}), block surface areas (A_{bl}) and ratios for block lengths (d_2/d_1).

		R2-2012			R1-2013			R2-2013			R3-2013		
		Av	Stdev	n	Av	Stdev	n	Av	Stdev	n	Av	Stdev	n
h_{bl}	(m)	0.87	0.08	6	0.48	0.11	22	0.40	0.10	45	0.26	0.06	69
d_1	(m)	1.49	0.66	6	0.94	0.29	10	0.97	0.45	43	0.94	0.65	41
d_2	(m)	1.83	0.63	6	1.41	0.59	10	1.35	0.63	45	1.30	0.77	47
α_{bl}	(°)	14.17	18.00	6	-	-	-	50.10	35.42	22	50.34	27.96	53
A_{bl}	(m^2)	2.97	2.29	6	1.43	1.07	10	1.54	1.41	43	1.71	2.45	41
d_2/d_1 (-)		1.30	0.50	6	1.52	0.37	10	1.49	0.50	43	1.55	0.53	41

Table 6. Correlation values of ridge geometry data including the total ridge height (H_S+H_K) and the ratios keel depth to sail height ratio (H_K/H_S), keel width to keel depth (W_K/H_K), keel width to sail height (W_K/H_S) and sail width to sail height (W_S/H_S).

	R1-2011[1]	R2-2011[3]	R2-2012[2]	R1-2013[3]	R2-2013[3]	R3-2013[3]	All data*	Svalbard*	Barents Sea*
$H_S + H_K$ (m)	7.10	9.30	7.40	5.40	8.90	9.90	8.90	6.10	10.00
H_K/H_S (-)	2.55	2.88	3.94	1.70	3.24	2.30	5.17	5.00	4.40
W_K/H_K (-)	8.63	4.63	2.99	9.41	4.71	8.42	4.85	-	-
W_K/H_S (-)	22.00	13.33	19.64	16.00	15.62	19.39	20.91	-	-
W_S/H_S (-)	4.00	3.75	8.48	7.00	5.85	3.03	3.75	-	-

*Average ridge data from Strub – Klein and Sudom (2012) for all first - year ridges, ridges in Svalbard regions and ridges in Barents Sea; [1] Ridge located in Svalbard region; [2] Ridge located in Fram Strait; [3] Ridges located in Barents Sea

Table 7. Average values for the ridge sail and keel macroporosity from different literature sources calculated from the given numbers of ridges (n_R) and bore holes (n_H).

	Macroporosity (%)			n_R (-)	n_H (-)
Source	Sail	Keel+CL	Keel	Ridges	Holes
Leppäranta and Hakkala (1992)	19	29	-	6	-
Beketsky et al. (1996)	26	-	28	1	-
Kankaanpää (1997)	20	30	-	8	-
Høyland (2007)	21	-	30	4	64[c]/189[d]
Kharitonov (2008,2012)	9	19	-	41	707
Ervik et al. (2018)	11 (22[a])	9	21	4	51
Present data	13 (19[a])	12 (15[b])	23 (30[b])	6	96[c]/182[d]

[a]Excluding sail porosities equal to zero [b]Excluding R1-2011 and R1-2013 [c]Sail [d]Keel

Table 8. Mean values for the minimum to average thickness (C_{Min}) and the maximum to average thickness (C_{Max}), the respective range of values from the studied ridges, the number of ridges and the ratio between C_{Max} and C_{Min}, being a measure for the variability of the consolidated layer thickness.

Source	C_{Max} (m)	Range (m)	C_{Min} (m)	Range (m)	n (-)	C_{Max}/C_{Min} (-)
Timco and Burden (1997)	1.68	1.2 … 2.7	0.51	0.1 … 0.9	25	3.3
Høyland (2002)	1.40	1.2 … 1.6	0.74	0.6 … 0.9	3	1.9
Høyland (2007)	2.00	1.6 … 2.6	0.38	0.3 … 0.7	4	5.3
Ervik et al. (2018)	1.98	1.8 … 2.3	0.39	0.2 … 0.6	4	5.1
Strub-Klein and Sudom (2012) – all ridges	3.75	-	0.19	-	117	20
Present data	2.24	1.5 … 3.1	0.19	0.0 … 0.5	5	11.6

Figure Captions

Fig. 1. Location of the six ridges studied from 2011 to 2013 (Sand et al., 2015)

Fig. 2. Example of a first-year ridge cross-section with characteristic dimensions.

Fig. 3. Photo (a) and cross-section (b) through the transect of ridge 1 measured in 2011.

Fig. 4. Photo (a) and cross-section (b) through the transect of ridge 2 measured in 2011.

Fig. 5. Profile along the spine (left) and transects B and C (right) of ridge R2-2012.

Fig. 6. Photos of ridges investigated in 2012 and 2013 which are ridges R2 – 2012 (a), R 1 – 2013 (b), R 2 – 2013 (c) and R 3 – 2013 (d).

Fig. 7. Transects along the spine (a) and through transect B (b) of ridge R1 -2013.

Fig. 8. Transects along the spine (a) and through transect B and C (b) of ridge R2-2013.

Fig. 9. Transects along the spine (a) and through transect B (b) of ridge R3-2013.

Fig. 10. Temperature profiles from ridges R1-2013 to R3-2013 and the adjacent level ice.

Fig. 11. Distribution of ice block thicknesses

Fig. 12. Possible ridge building process for R3-2013, showing the initial situation (a), the rafting and ridging of the lead ice and level ice (b) and the ridges transect B at date of investigation (c). Enlargements of pictures from the crystal studies show examples for ice texture at different ridge locations. The greyed out area marks a zone in the ridge keel that contains mainly crushed ice.

Fig. 13. Ice drift tracks iterated from (a) NCEP and (b) ERA wind data shown from 1st of January to 29th of April 2013. The zones of likely ridge formation place are marked by a double arrow. (c) Daily quiver plots for ice drift generated by CERSAT/IFREMER. Ice drift trajectories represent ice drift for 6 days periods respectively.

Fig. 14. Air temperatures along the drift track from January to April 2013.

Fig. 15. Wind speeds 10 m above surface along the drift track from January to April 2013. The time periods for possible ridge formation calculated from ERA-Interim and NCEP data are sketched in the figure.

Fig. 16. Expected pressure ridge formation date in 2013 (a) backwards calculated from FDD models. The horizontal dotted line marks the level ice thickness at R3-2013, i.e. the intersections with the curve indicate the predicted ice formation date. Two time intervals for the respective temperature dataset were obtained. (b) The possible ridge formation date based on the block size thickness (horizontal dotted line).

Fig. 17. The ratios of ice block thickness and sail height vs. the sail macro porosity.

Fig. 18. Macroporosity vs. depth, from water level downwards in 0.5 m steps. Dashed lines show the macroporosity calculated from varying number of boreholes with depth and grey, solid lines show the number of boreholes available at each depth.

Fig. 19. Distribution for ratios of block dimensions d2/d1

Fig. 20. Cumulative distribution of block dimension ratio d2/d1

Fig. 21. Block dimension ratio d_2/d_1 for different ice block thicknesses

Fig. 22. Cumulative frequency for ratios of block dimensions d_2/h_{bl} from the measured ridges in 2012 and 2013

Fig. 23. Cumulative frequency for ratios of block dimensions d_2/h_{bl} of all present block measurements and data from literature.

Fig. 24. Lognormal QQ-plot for ratios d_2/h_{bl}

Figures

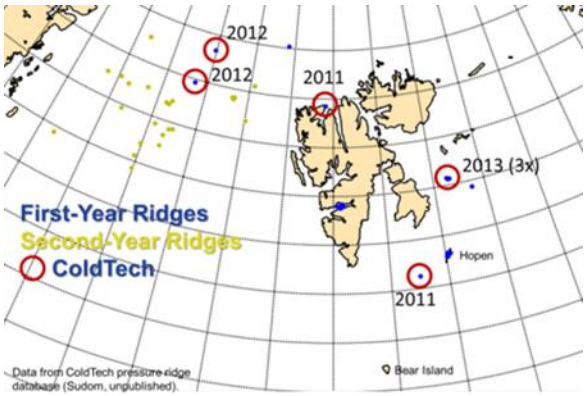

Fig. 2. Location of the six ridges studied from 2011 to 2013 (Sand et al., 2015)

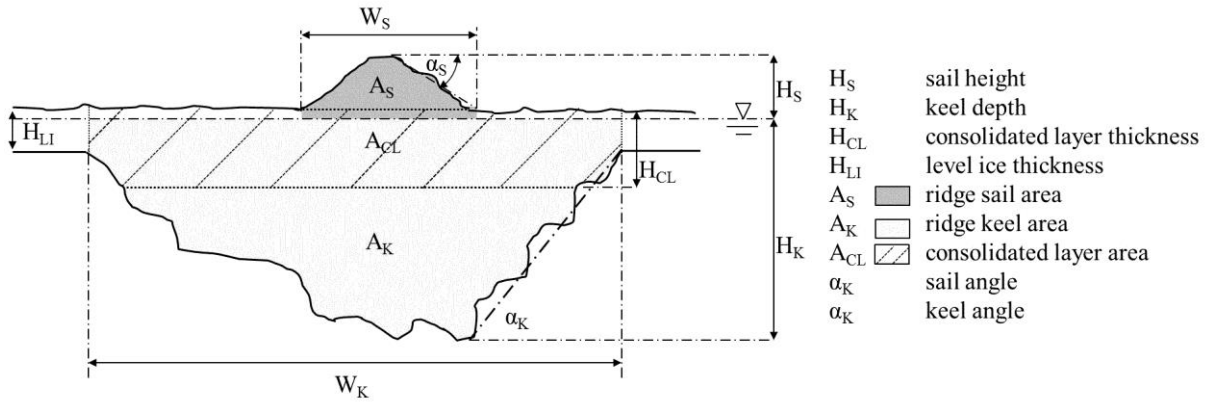

Fig. 2. Example of a first-year ridge cross-section with characteristic dimensions.

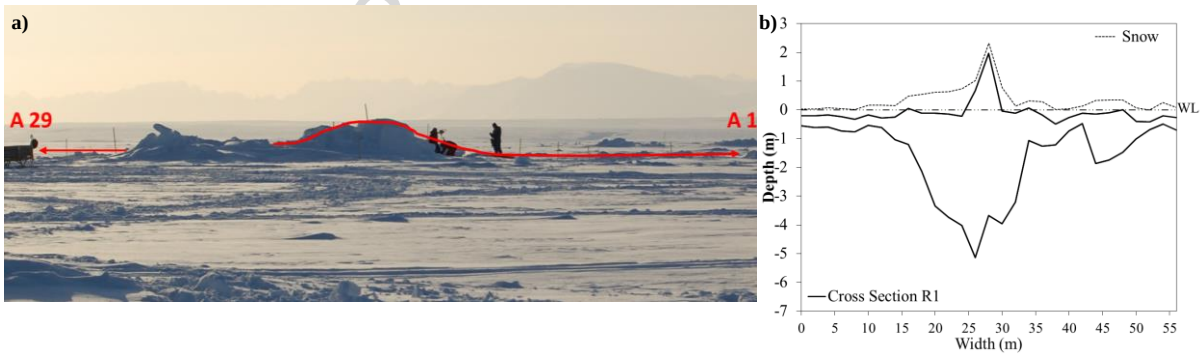

Fig. 3. Photo (a) and cross-section (b) through the transect of ridge 1 measured in 2011.

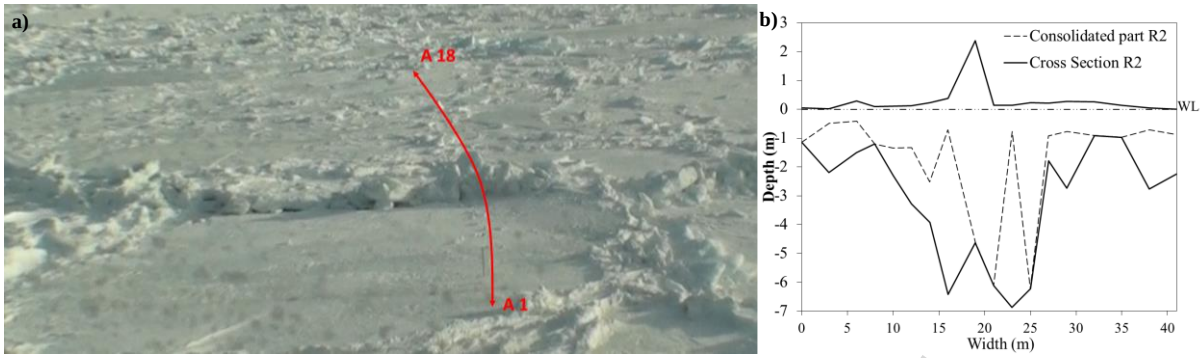

Fig. 4. Photo (a) and cross-section (b) through the transect of ridge 2 measured in 2011.

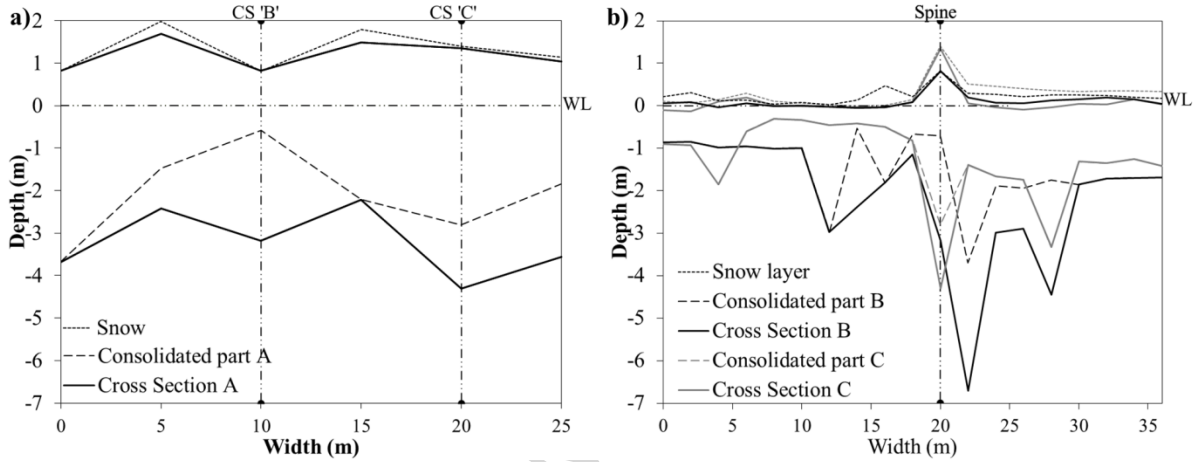

Fig. 5. Profile along the spine (left) and transects B and C (right) of ridge R2-2012.

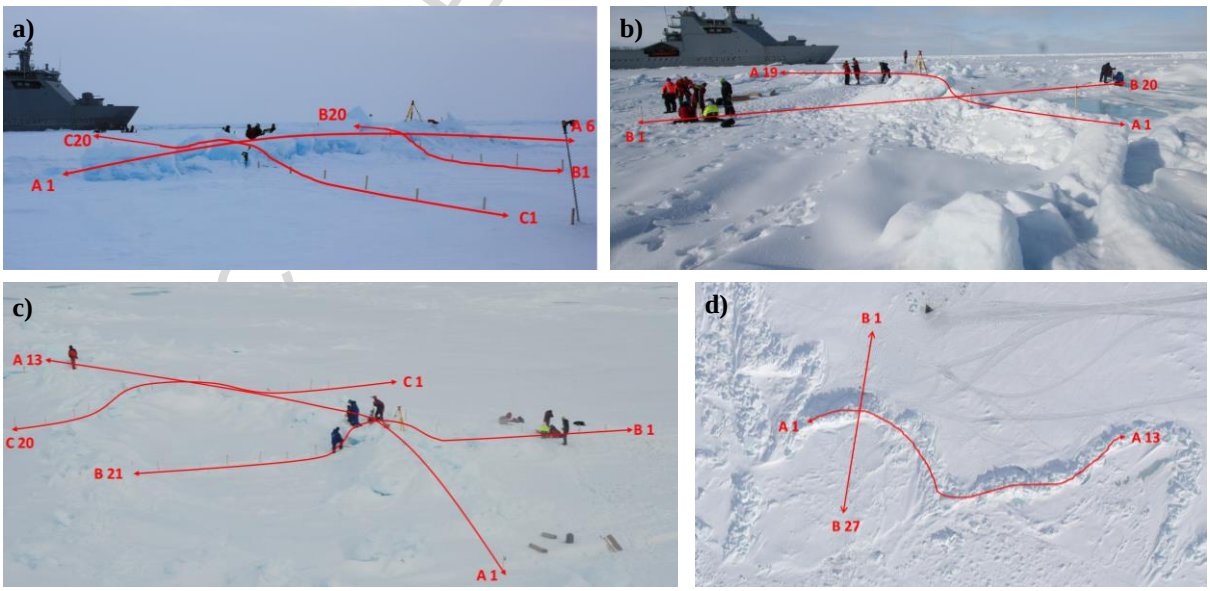

Fig. 6. Photos of ridges investigated in 2012 and 2013 which are ridges R2 – 2012 (a), R 1 – 2013 (b), R 2 – 2013 (c) and R 3 – 2013 (d).

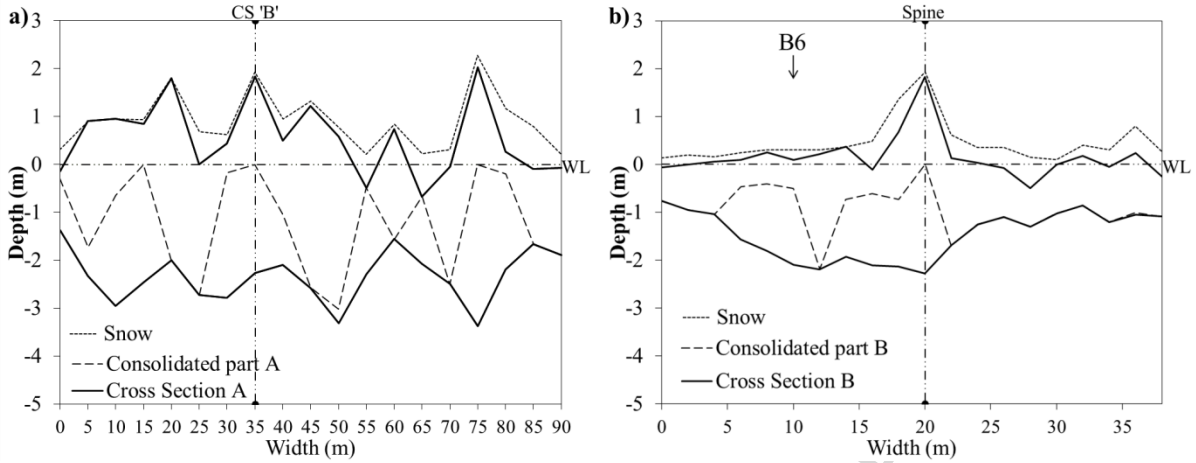

Fig. 7. Transects along the spine (a) and through transect B (b) of ridge R1 -2013.

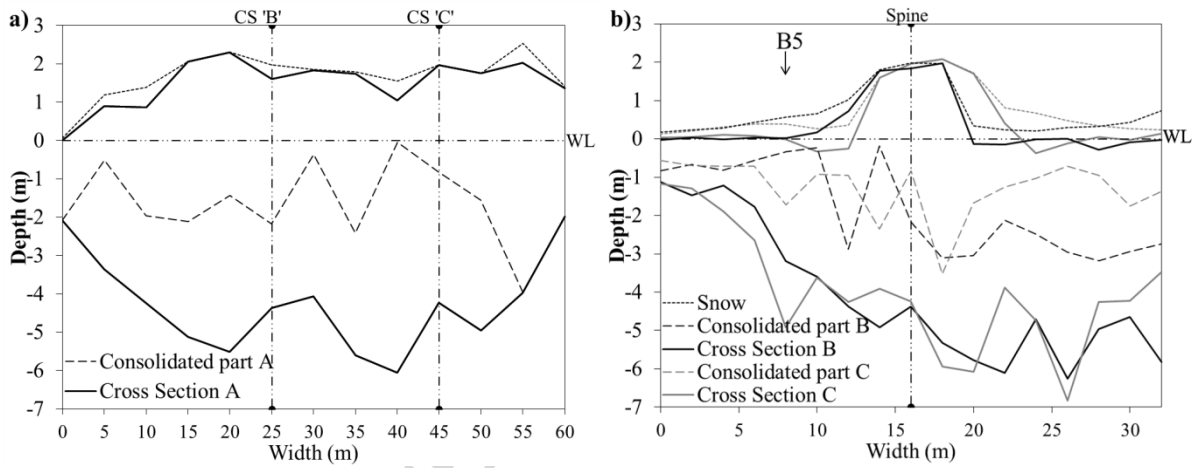

Fig. 8. Transects along the spine (a) and through transect B and C (b) of ridge R2-2013.

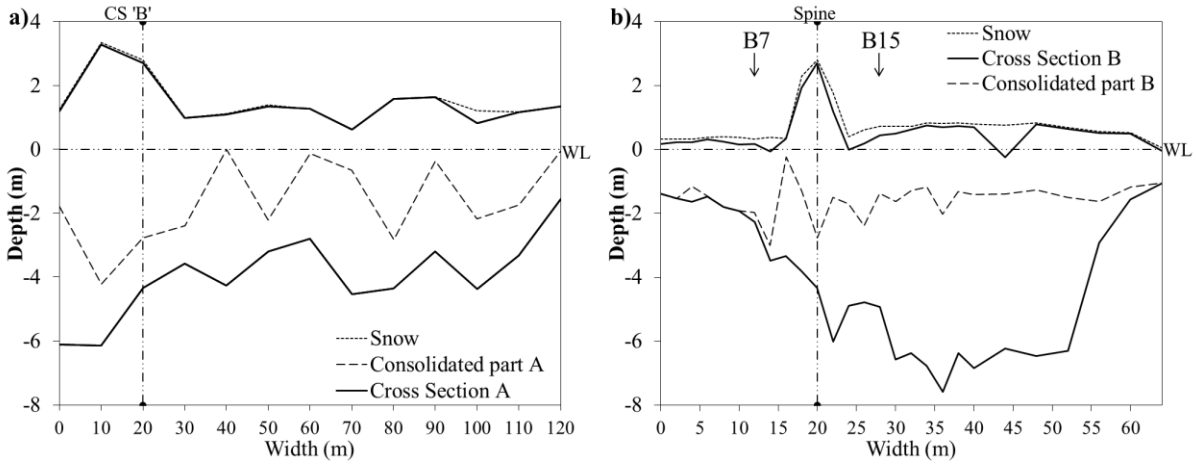

Fig. 9. Transects along the spine (a) and through transect B (b) of ridge R3-2013.

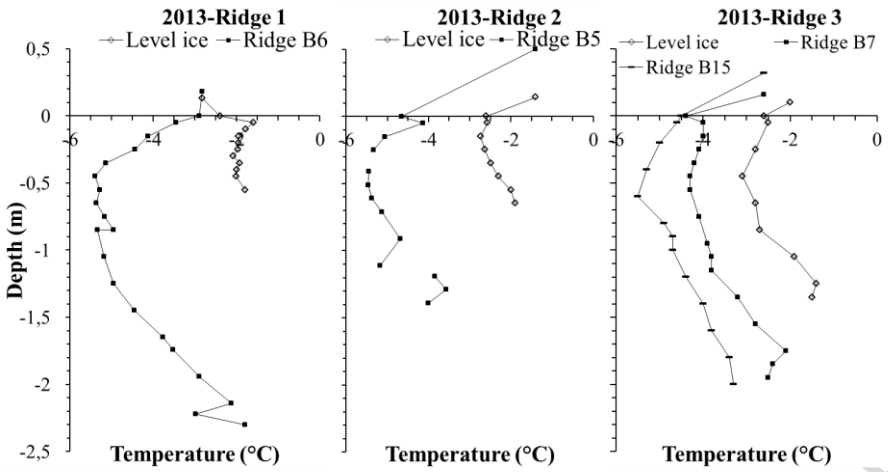

Fig. 10. Temperature profiles from ridges R1-2013 to R3-2013 and the adjacent level ice.

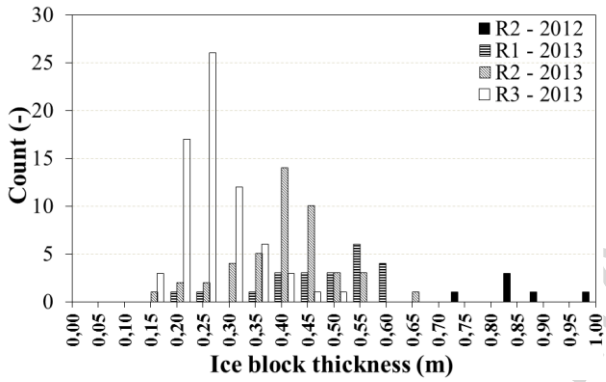

Fig. 11. Distribution of ice block thicknesses

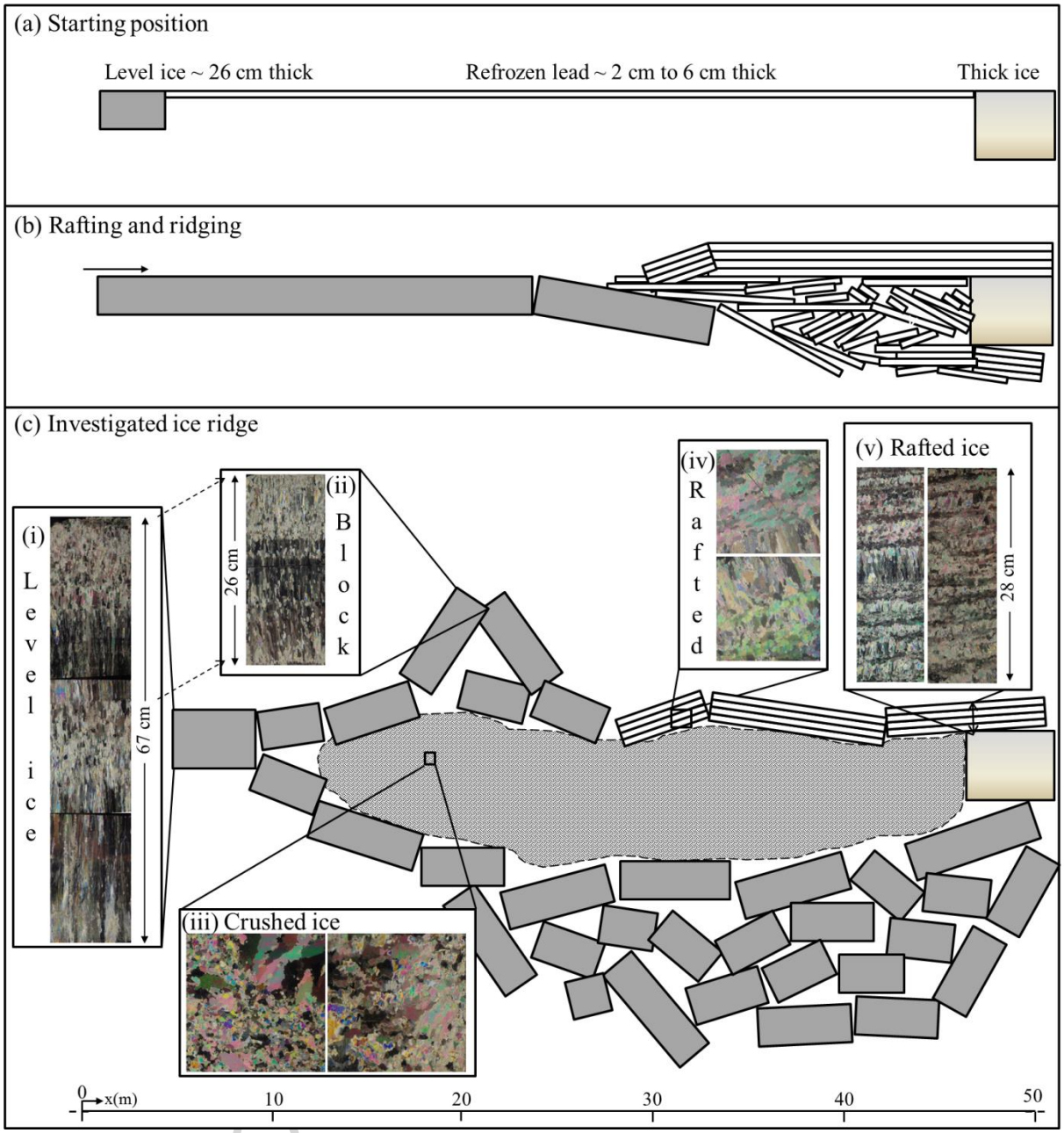

Fig. 12. Possible ridge building process for R3-2013,showing the initial situation (a), the rafting and ridging of the lead ice and level ice (b) and the ridges transect B at date of investigation (c). Enlargements of pictures from the crystal studies show examples for ice texture at different ridge locations. The greyed out area marks a zone in the ridge keel that contains mainly crushed ice.

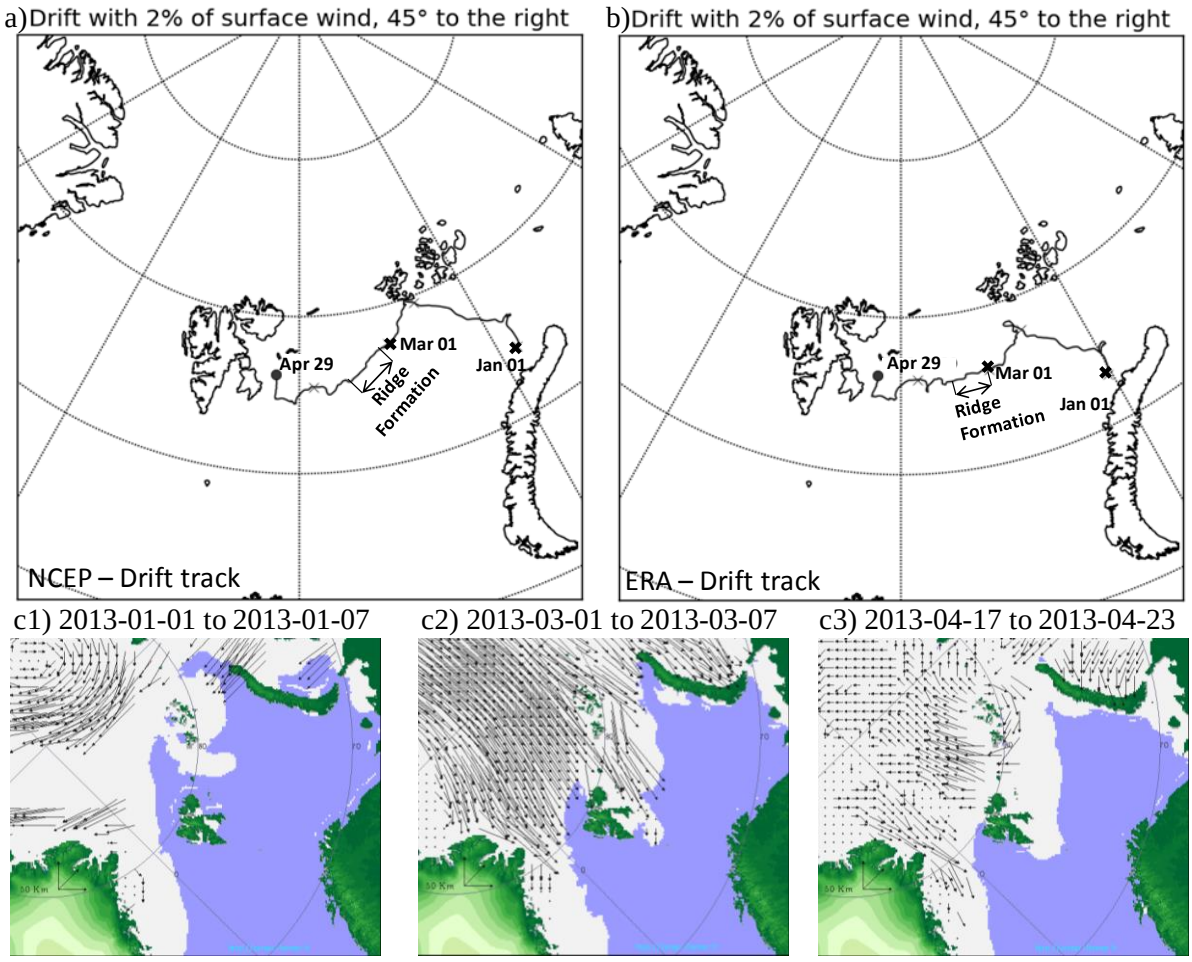

Fig. 13. Ice drift tracks iterated from (a) NCEP and (b) ERA wind data shown from 1st of January to 29th of April 2013. The zones of likely ridge formation place are marked by a double arrow. (c) Daily quiver plots for ice drift generated by CERSAT/IFREMER. Ice drift trajectories represent ice drift for 6 days periods respectively.

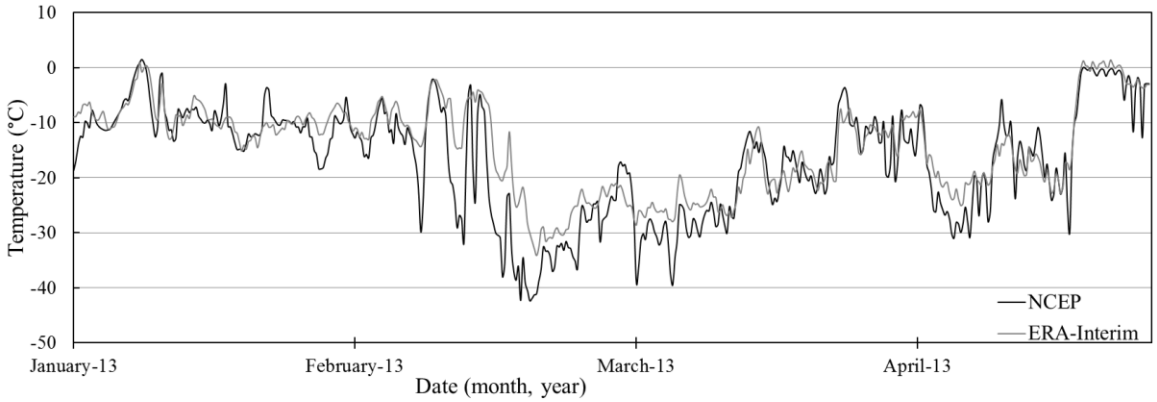

Fig. 14. Air temperatures along the drift track from January to April 2013.

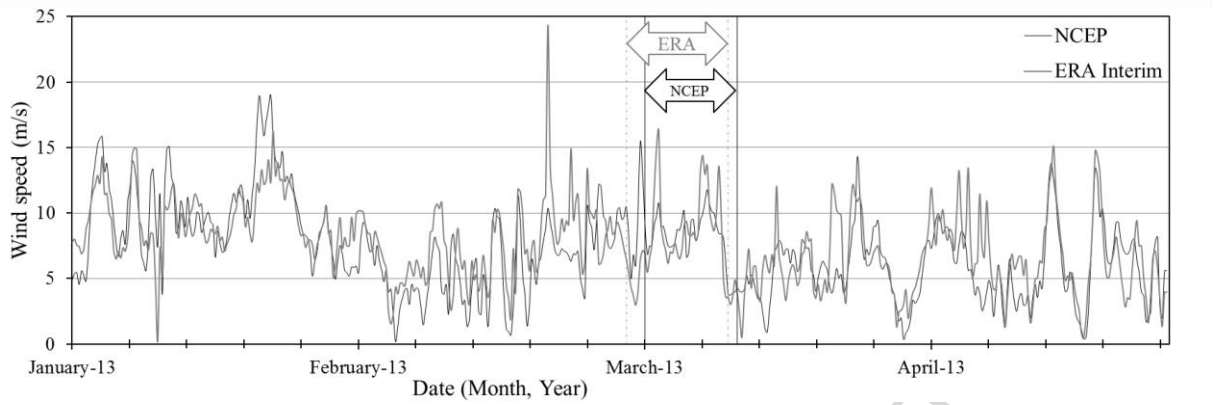

Fig. 15. Wind speeds 10 m above surface along the drift track from January to April 2013. The time periods for possible ridge formation calculated from ERA-Interim and NCEP data are sketched in the figure.

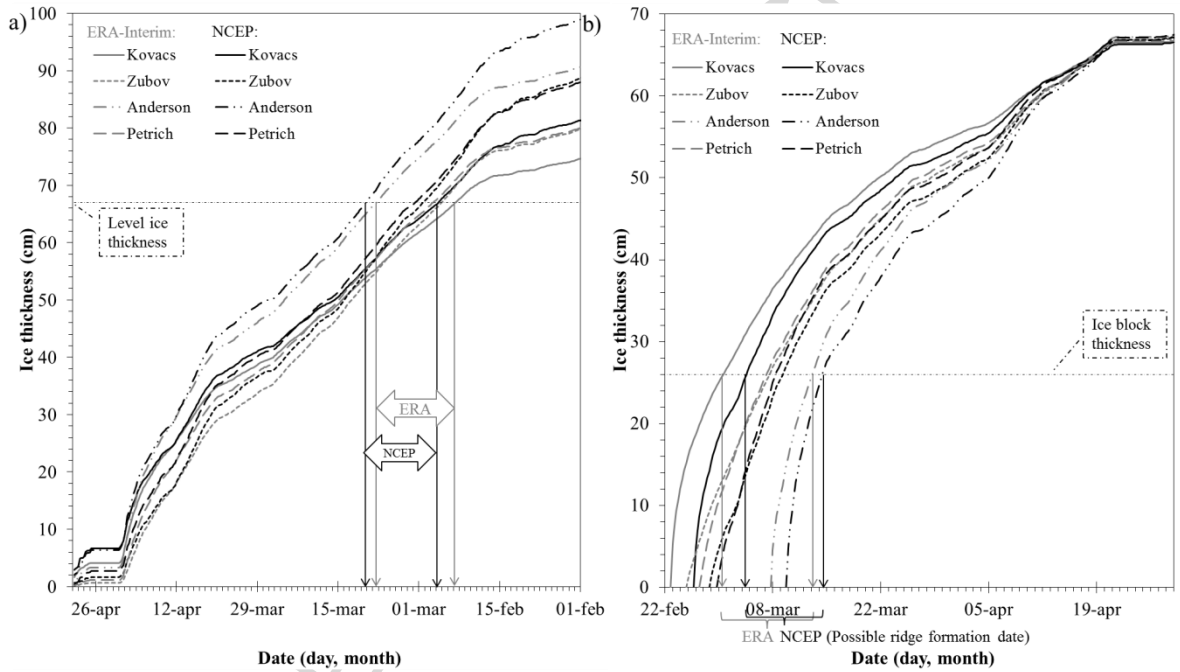

Fig. 16. Expected pressure ridge formation date in 2013 (a) backwards calculated from FDD models. The horizontal dotted line marks the level ice thickness at R3-2013, i.e. the intersections with the curve indicate the predicted ice formation date. Two time intervals for the respective temperature dataset were obtained. (b) The possible ridge formation date based on the block size thickness (horizontal dotted line).

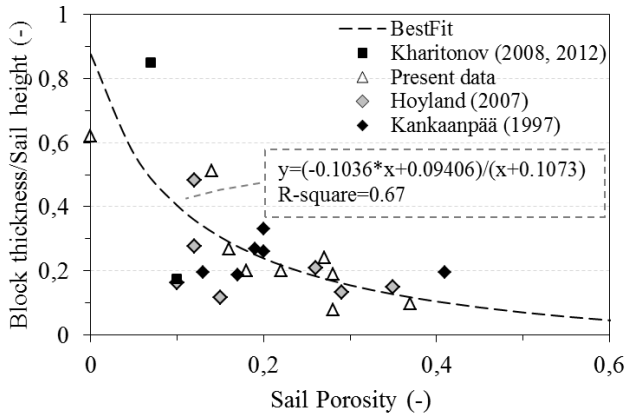

Fig. 17. The ratios of ice block thickness and sail height vs. the sail macro porosity.

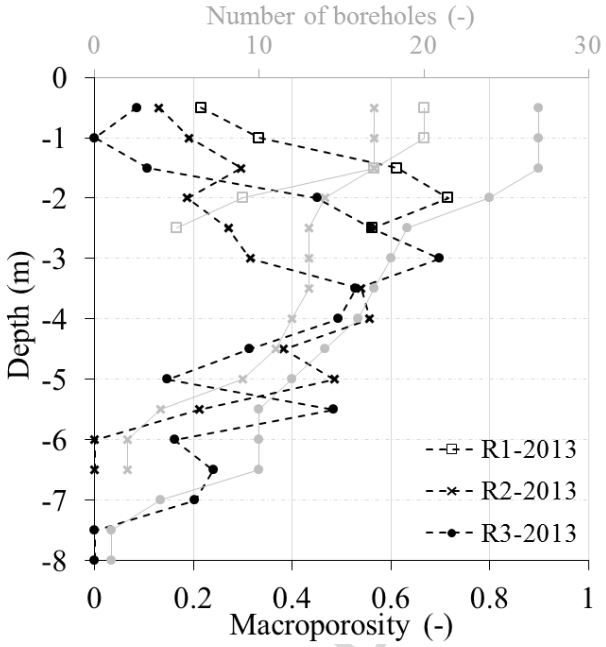

Fig. 18. Macroporosity vs. depth, from water level downwards in 0.5 m steps. Dashed lines show the macroporosity calculated from varying number of bore holes with depth and grey, solid lines show the number of boreholes available at each depth.

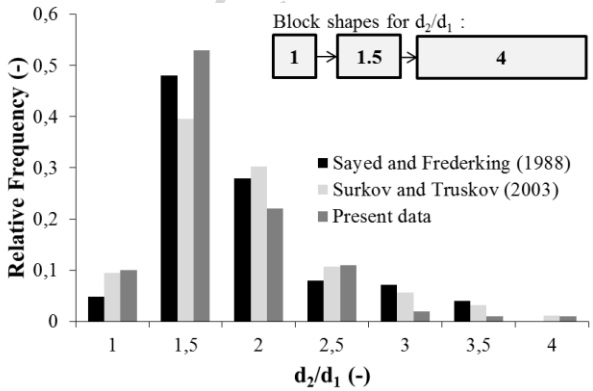

Fig. 19. Distribution for ratios of block dimensions d2/d1

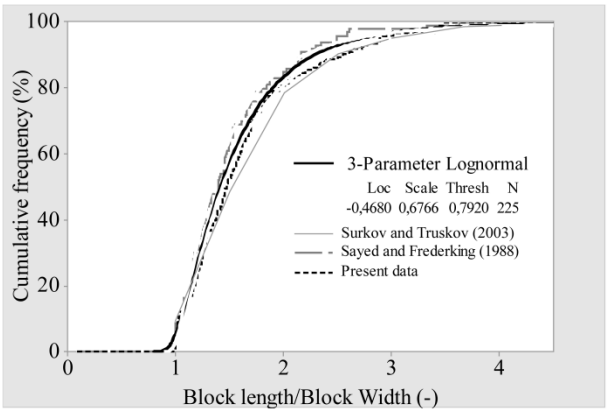

Fig. 20. Cumulative distribution of block dimension ratio d2/d1

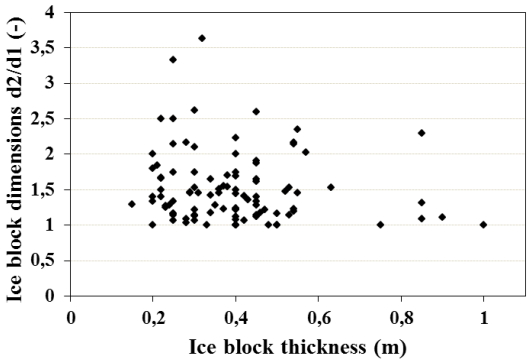

Fig. 21. Block dimension ratio d_2/d_1 for different ice block thicknesses

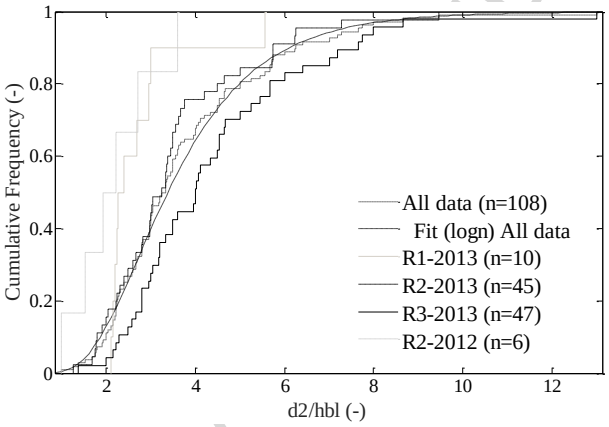

Fig. 22. Cumulative frequency for ratios of block dimensions d_2/h_{bl} from the measured ridges in 2012 and 2013

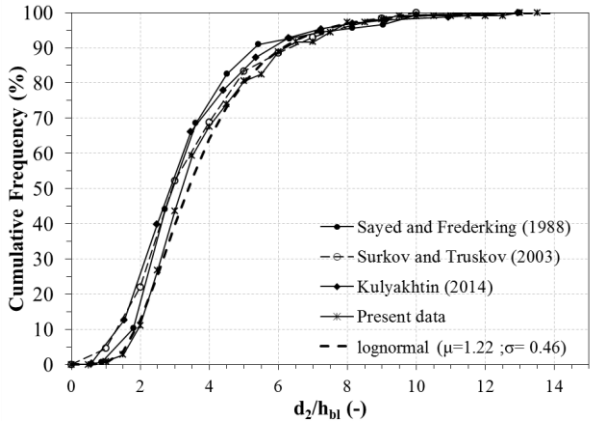

Fig. 23. Cumulative frequency for ratios of block dimensions d_2/h_{bl}.all present block measurements and data from literature.

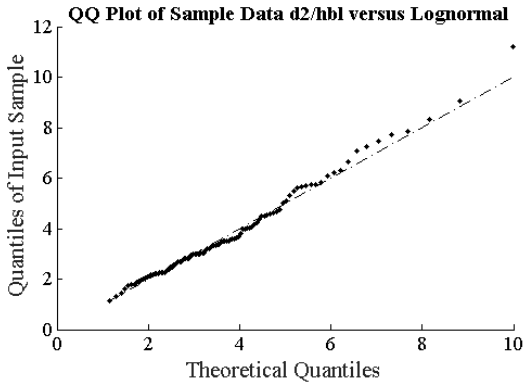

Fig. 24. Lognormal QQ-plot for ratios d_2/h_{bl}

Highlights:

- Data from field measurements on in total 6 first-year ice ridges are presented
- Ice block size and shape distribution appears predictable
- Ridge keel consolidation ranges from 30 % to 90 % of the ridge keel
- Ridge formation process can be reproduced from field data and reanalysis products